UCRL-50016-77-4

MECHANICAL ENGINEERING DEPARTMENT QUARTERLY REPORT
October through December 1977

Scientific Editor: R. G. Stone
General Editor: M. B. Bathgate

December 31, 1977

Work performed under the auspices of the U.S. Department of Energy by the UCLLL under contract number W-7405-ENG-48.

Printed in the United States of America
Available from
National Technical Information Service
U.S. Department of Commerce
5285 Port Royal Road
Springfield, VA 22161
Price: Printed Copy $; Microfiche $3.00

Page Range	Domestic Price	Page Range	Domestic Price
001-025	$ 4.00	326-350	$12.00
026-050	4.50	351-375	12.50
051-075	5.25	376-400	13.00
076-100	6.00	401-425	13.25
101-125	6.50	426-450	14.00
126-150	7.25	451-475	14.50
151-175	8.00	476-500	15.00
176-200	9.00	501-525	15.25
201-225	9.25	526-550	15.50
226-250	9.50	551-575	16.25
251-275	10.75	576-600	16.50
276-300	11.00	601-up	[1]
301-325	11.75		

[1] Add $2.50 for each additional 100 page increment from 601 pages up.

LAWRENCE LIVERMORE LABORATORY
University of California Livermore, California 94550

UCRL-50016-77-4

MECHANICAL ENGINEERING DEPARTMENT QUARTERLY REPORT October through December 1977

Scientific Editor: R. G. Stone
General Editor: M. B. Bathgate

MS. date: December 31, 1977

CONTENTS

MECHANICAL ENGINEERING DEPARTMENT QUARTERLY REPORT October through December 1977

INTRODUCTION

This issue of the *Mechanical Engineering Department Quarterly Report* is devoted to the activities of the Materials Engineering Division (MED). This Division provides complete technical services for mechanical and thermophysical characterization of materials and components, and for inspection, evaluation, and proof testing of complete systems. MED is composed of approximately 170 people who contribute to the engineering, design, procurement, assembly, and operation of testing systems. Their efforts are directed toward making valid engineering/scientific measurements in support of Laboratory programs and in advancing their expertise through an active program of research and development. The Division has more than 20 separate laboratories and facilities, which are organized into 7 sections. The activities of each section are described below.

Engineering Design

This section designs and fabricates component and system hardware for the Chemistry and Materials Science Department, the Earth Sciences Division, and MED itself. A major effort is support of the Tritium Facility operation by designing tritium-handling systems, directing associated quality-assured upgrading activities, and developing tritium-certified hardware. An ongoing research program studying hardware safety is described on page 2 in this issue.

Engineering Measurements

This section provides various kinds of measurements engineering to Laboratory programs, ranging from the calibration of a single transducer to the fielding of complete measurement systems. Service for the calibration and installation of conventional pressure and force transducers and accelerometers is available. In addition, more sophisticated transducers can be developed that will serve in hostile environments, such as severe shock, temperature, or radiation fields. A unique application of foil strain gages operating to 4.2 K in a 12-T field is presented on page 9. The section also has a highly automated facility for measurement of thermophysical properties of materials, e.g., conductivity, specific heat, diffusivity, and thermal expansion.

High Pressure

The High Pressure Section provides the necessary technology and facilities for conducting high-pressure gas and liquid experiments. The personnel are also responsible for providing certified and safe tubing, valves, fittings, and miscellaneous hardware for use in tritium-handling systems. Remote, explosion-safe test cells are maintained for programmatic use, research and development, and periodic proof testing of standard hardware as part of the Lab-wide Quality Assurance Program. High-temperature gas autoclaves are used for diffusion bonding studies and compaction sintering or densification research.

Materials Test and Evaluation

This section maintains up-to-date capabilities to provide mechanical testing through application of ASTM standard tests and to conduct special test procedures tailored to individual customer requirements. A high level of engineering and technical expertise is directed at continuing development in the special fields of acoustic emission, fracture mechanics, high-rate response, and composite materials evaluation. Part of our long-range program in the evaluation of fiber composite pressure vessels is the study of the micromechanical failure mechanisms. Acoustic emission technology is being used (see page 13) in the evaluation of composites. Facilities are also available for photoelasticity, high-explosive characterization, and soil mechanics testing. A complete line of auxiliary equipment allows work in thermal environments from 4.2 to 2300 K in vacuum, corrosive environments with loading combinations of tension, compression, torsion, and internal pressure.

Nondestructive Evaluation

The engineers and technicians in this section provide quality-assurance services and engineering inspections for LLL programs. The work requires extensive liaison and field operations throughout the Department of Energy agencies and field testing centers. Nondestructive evaluation is done with neutron, x-ray, gamma, source radiography, ultrasonics, eddy current, dye penetrant, and magnetic particle techniques. Precision radiation gaging is available using both through-transmission techniques as well as various backscattering approaches when only one surface is readily available. Holographic interferometry is used to study deformations resulting from changes in applied stress levels. Major efforts are directed to advancing the state of the art in ultrasonic and holographic techniques and applying the knowledge to meet the exacting requirements of LLL programs.

Plutonium Engineering

The Plutonium Facility is jointly operated by MED and the Metals and Ceramics Division of the Chemistry and Materials Science Department. The engineering activities are readily grouped into two separate efforts: (1) engineering design, fabrication, and execution of testing in support of Chemistry Programs, and (2) direct Weapons Program support by fabrication of device hardware and complete responsibility for component tests and evaluations. In addition, the section is responsible for quality-assurance activities and safety programs within the hazardous area of the Plutonium Facility building. Maintenance, modification, and upgrading of the complex box lines, internal tools, and equipment are handled on a daily basis.

Research and Advanced Development

This section is composed of personnel with broadly based technology expertise. Their expertise ranges from the design and fielding of computer-based data acquisition and control systems such as the T-DAC (page 21) to research on laser beam/material interactions. Comprehensive studies are carried out under the Mechanical Engineering Research Program with long-range goals of supporting the Nuclear Explosives Program. Another major effort is support of the Weapons Division's environmental testing activities by designing and developing data and control systems. Reimbursable programs are coordinated through this section in order to provide an interdisciplinary team approach to complex and difficult projects. Joint research efforts with H-Division, Chemistry and Materials Science Department, and D-Division are currently being pursued. Elastic constraints are being measured at temperatures above melt (see page 26) in a joint project with Physics.

MATERIALS COMPATIBILITY STUDY OF 316 STAINLESS STEEL AT THE LLL TRITIUM FACILITY

We are conducting an experimental test series to investigate the stress corrosion rate of nuclear grade 316 VIM/VAR stainless steel. The experiment was initiated three years ago in response to the Quality Assurance requirements of the Tritium Facility's Safety Upgrading Program. This program was begun in 1971 to upgrade the tritium handling systems by using improved materials and fabrication techniques to decrease the probability of a tritium release. [1]

As part of the program, the high-pressure gas system was redesigned at the Tritium Facility. The valves in this system contain Teflon as a valve packing material. Such valves have worked satisfactorily at LLL for years. However, it is known that Teflon breaks down when subjected to tritium radiation and the radiolysis produces either halide compounds or radicals. [2] In the presence of halide-water mixtures, 18-8 austenitic stainless steels (such as nuclear grade 316) are subject to severe stress corrosion attack. [3] This is of concern since the high-pressure tritium gas system has all the necessary components—an intense radiation field, Teflon, small amounts of water, and nuclear grade 316 stainless steel. Thus, the Quality Assurance Program requires that either calculations be made to show the systems will not fail; or if this is not possible, a suitable testing program should be performed to ensure against failure. The experimental test was chosen since the necessary information on tritium exposure was not available. We were charged with conducting tests that produce adequate, applicable, convincing, conclusive, and not excessively expensive results. This work was performed by the Materials Engineering Division in support of the Chemistry and Materials Science Department.

Experimental Plan

We set up an experiment using 32 small pressure vessels made from 316 stainless steel and loaded with corrosive agents, water, and Teflon in a statistically designed matrix. These vessels were pressurized to different stresses using deuterium or tritium as the pressurizing gas. The experiment was planned in two phases. The first phase was an exploratory effort to test the corrosive effects under varying conditions. In the second phase, currently underway, we have used the results of the first phase to choose tests to refine and expand our results.

The 32 specimens are secondarily contained in 16 cans to reduce costs. The initial specimens can be replaced with second specimens, allowing the reuse of the secondary container and valves in Phase 2.

Table I lists the conditions for our Phase I experiments. Note that 28 samples contained deuterium gas and 4 contained tritium. Tritium was used in Phase I to gain some insight into the more complicated tritium effects to be investigated in Phase 2. For all tests, we held temperature at a constant 100°C to accelerate the expected room temperature reaction, used 500 ppm of water, and used either tritium or deuterium as the pressurizing gas. Presence of Teflon, internal notching, and level of stress were variables. Some samples had an internal Electric-Discharge Machining (EDM) notch as a "stress concentrator" variable. Stress levels of 100%, 90%, and 80% of yield were used. For 24 of the tests, known amounts of HF and H_2S were added as corrosive agents to account for the possible presence of fluorides and sulfides in the actual high-pressure gas system.

Our original plan was to run the experiment for 9 months. If the specimens did not break or leak in that time, they would be depressurized and either sectioned and metallurgically examined or repressurized and run to burst.

Table I. Phase 1 stress corrosion experiment. A total of 32 samples were tested at 100° C and 137.8 MPa.

Sample chemical contents	Teflon used	Number of samples	
		Notch	No notch
$D_2 + H_2S + H_2O$	X	3[a]	3
$D_2 + H_2S + H_2O$	—	3	3
$D_2 + HF + H_2O$	X	3	3
$D_2 + HF + H_2O$	—	3	3
$D_2 + H_2O$	X	2[b]	–
$D_2 + H_2O$	—	2	–
$T_2 + H_2O$	X	2	–
$T_2 + H_2O$	—	2	–

[a]When three samples of the same type were used, stress levels were 1.0, 0.9, 0.8 of yield.

[b]When two samples of the same type were used, stress levels were 1.0 and 0.8 of yield.

Experimental Apparatus

Test Specimen Design. The specimens (Fig. 1) are made from 9/16-in. o.d., 5/16-in. i.d. VIM/VAR tubing, MEL-71-001150G. The tubes are necked down to a 0.76-mm wall thickness. This gives an internal hoop stress of approximately 689.3 MPa, which is at or above the yield point of half-hard 316 VIM/VAR stainless steel.

After the tubes were machined, six units were each tested with an internal strain gage and two external strain gages. All gages measured stress in the hoop stress direction. The pressures were increased 6.8 MPa per run from a base of 68.9 MPa, held for 5 min, and slowly released. These tubes burst at 186.1 to 193.0 MPa. The results showed good uniformity among the six specimens throughout the pressure ranges.[4] The deviation of the internal pressure-plastic strain history envelope among the different tubes was small. This data will be used to compare with the exposed specimens. When used, the stress concentrating notch is 0.025 mm deep, 0.025 mm wide, and 6.35 mm long running axially.

Secondary Container Design. Since the specimens will either leak down or burst, an adequate secondary container is required to contain the total gas load. The container (Fig. 1) has shrapnel shields (to protect one specimen and its instrumentation from the rupture of its mate), an electrical feedthrough, double valve (to protect against across-the-seat leaks), a pump out port, pressure gage, valve, and pump out connection. The container is designed to have minimum volume in its high-pressure assembly to minimize the amount of tritium required. The outer high-pressure valve is removable complete assembly (container and specimens) is fabricated, inspected, and documented to the standards of the high-pressure gas handling systems.

High-Pressure Gas Transfer System. Since corrosives are added to the containers before the loading of the high-pressure gas, a separate gas loading system was required. The system (Fig. 2) is designed to load four containers (eight specimens) per run and then to be followed by one cleanup run

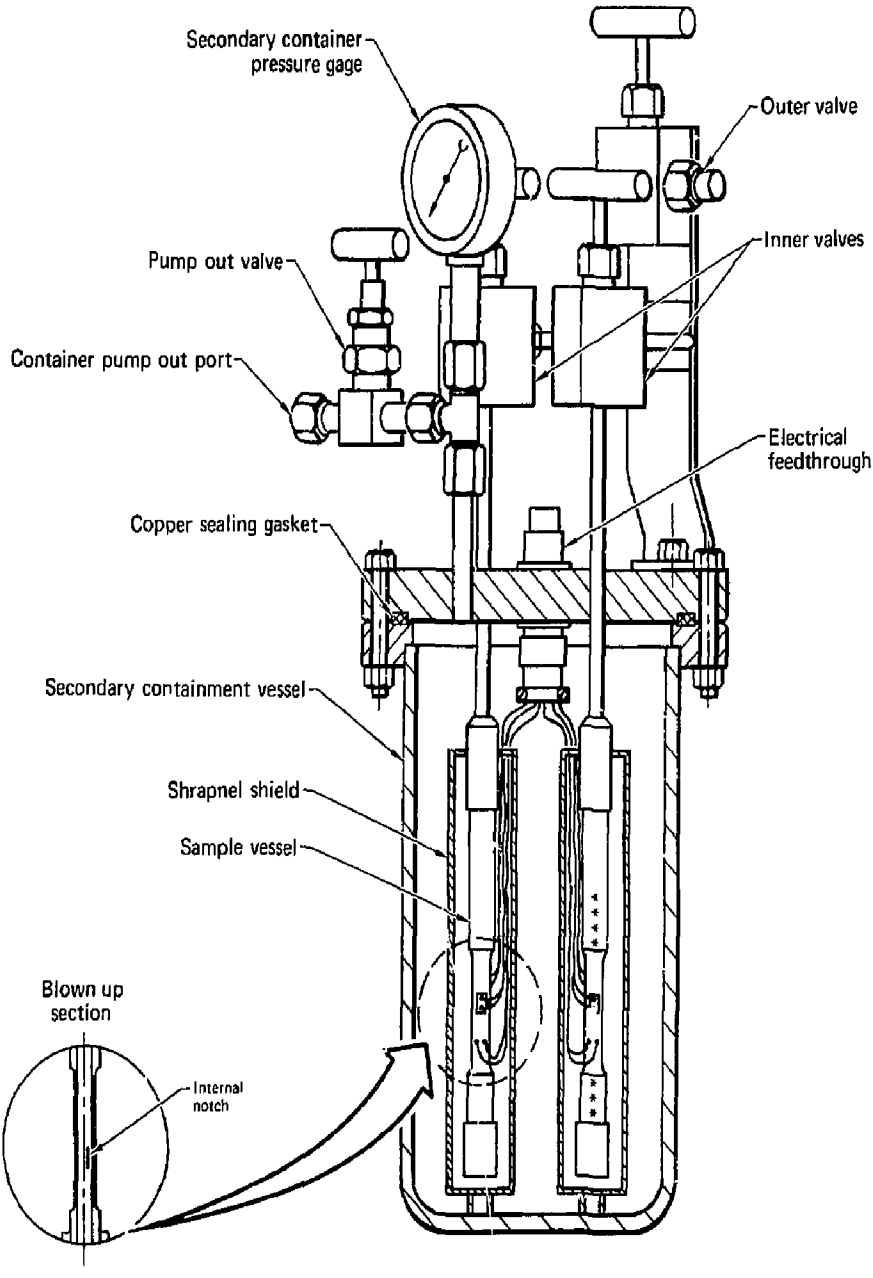

Fig. 1. Specimen containment vessel.

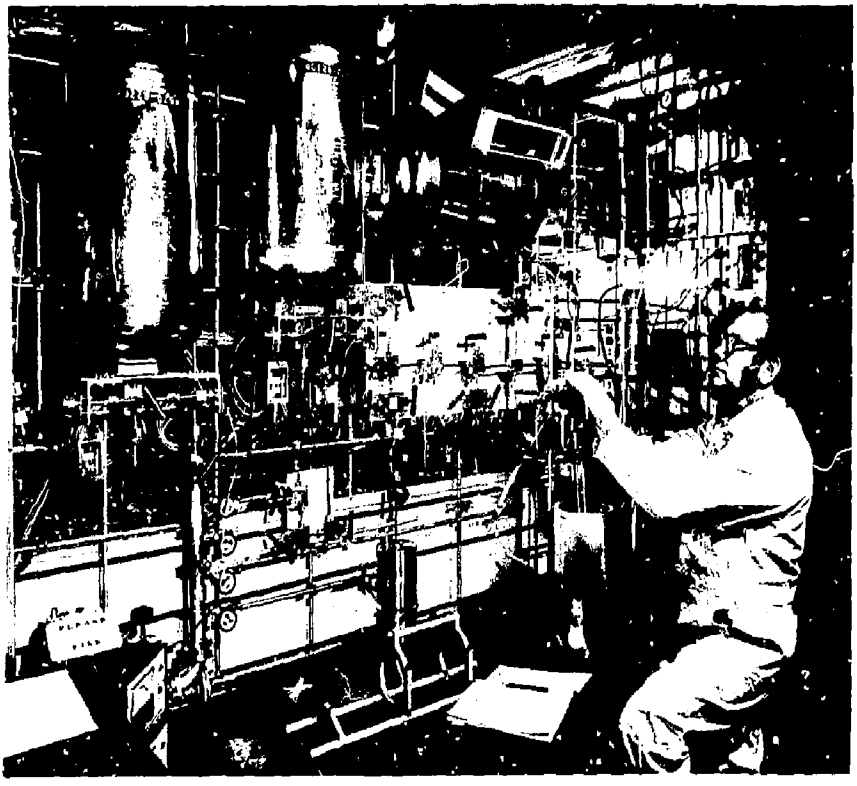

Fig. 2. High-pressure gas transfer system.

(flushing the system with helium). The system consists of a secondarily contained high-pressure transducer and its abort can, a high-pressure gas manifold, two recovery tanks (for scavaging the system), a high-pressure helium flushing system, and a vacuum system. The high-pressure gas capillary lines (AAA74-114312-00) and the transfer vessels and cryovessels are not considered part of the system but are separate subassemblies.

Instrumentation. The instrumentation consists of two strain gages in the hoop stress direction and one iron constant thermocouple per specimen. These are read by a computer program via a 100-channel scanner and an integrating digital voltmeter.

Associated Equipment. Associated equipment designed included: a water and corrosive agent loading system, three high-pressure cryovessels, and a thermally controlled bath.

Experimental Procedure

After the specimens are tested and strain gaged, those that include Teflon in their test have about 1 g of Teflon chips inserted and weighed. All specimens are then threaded on the nipples of the secondary container and welded. The thermocouple and strain gages are connected, and the unit is pressurized to 137.8 MPa with deuterium or with a helium-10% oxygen mixture to set the yield point. This stresses the tube and exercises the strain gages. The gage readings are recorded and retained for post-experimental comparison. Next, the water and corrosive agents are added to the specimen and frozen out with liquid nitrogen. The units are placed in the bath and brought to thermal equilibrium. The gas is then loaded into them using the gas transfer system.

After the units have failed, samples of the gas are removed (preferably from the inner container) and the unit is flushed with helium and then evacuated. Mass spectrometric and gas chromatographic analyses are run on the gas sample. The assembly is removed from the bath and disassembled in a hood. Sections are removed for examination, including metallurgical, scanning electron microscope, Auger,

and microprobe analyses. Those that survive the prescribed time limit may be pressurized to burst or simply be sectioned and examined in the same manner.

Phase 1 Results

The 28 deuterium samples and 4 tritium samples were loaded at 137.8 MPa in May 1977 (see Table 1). The two tritium samples with Teflon and water failed at 11 and 16 h. The other two samples with tritium and water are still running as are all the deuterium samples.

The failed specimens were removed, sectioned, and examined metallurgically. Intergranular corrosion cracking was extensive as shown by Fig. 3, a scanning electron microscope photograph. The quantities and nature of alloys, elements, and compounds on the inside of the tubes are presently being investigated by the Chemistry and Materials Science Department.

The deuterium specimens have shown no outward sign of corrosive attack and the strain gage instrumentation continues to look normal after 4 months of loading near or at the yield point.

Phase 2 Test Series

The early failures were not anticipated, so we instituted a Phase 2 test series. We decided to allow the other samples to run and to immediately replace the failed specimens with two new ones and to reload the two companion specimens (which fortunately contained Teflon chips). All four specimens were loaded with tritium, Teflon, and water. They were loaded to 137.8, 110.3, and 82.7 MPa to verify the previous results and to extend the pressure range to a lower value.

Fig. 3. Example of intergranular stress corrosion (1000×).

Since the original specimens at 137.8 MPa failed so quickly, the lower 82.7-MPa pressure was chosen as a point further away from an "accelerated test" and closer to the normally encountered stresses. It is also of critical importance to determine if there is a pressure (stress) and tritium concentration effect on the failure mechanism.

Phase 2 Results

The 137.8- and 110.3-MPa specimens failed at 16 h 12 min and 25 h 40 min, respectively, after tritium pressurization, thus verifying the first two tritium-induced failures. The 82.7-MPa specimens failed at 30 h 59 min and 31 h 32 min after tritium pressurization. Table 2 summarizes the tritium tests performed and the type of failure. The specimens failed either by developing a leak or by blowing out a section under extreme stress (catastrophic failure). Usually the higher pressurized specimens failed by a slow leak and a ductile dimple to the surface, while the lower pressure specimens failed catastrophically.

The failed assemblies were sampled for gas analyses, depressurized, and decontaminated. The mass spectrometric analysis showed no unusual results, but the chromatographic analysis run on these samples showed $C(H,T)_4$ concentrations on the order of 300^{+} ppm.

Visual examination of all the failed specimens showed extensive i.d. surface cracking (Fig. 4). Scanning electron microscope examination showed extensive intergranular stress corrosion cracking (Fig. 5). The failed sections showed intergranular cracking on the i.d. surface leading to an abrupt ductile failure. The EDM notches played no role in the tube failures. As shown in Fig. 6, time to failure appears to vary directly with applied stress and tritium concentration.

The shredded Teflon showed no apparent discoloration or change from the original condition. Qualitative calculations set the Teflon and metallic i.d. surface doses at 10^{3} rad/s and 5×10^{2} rad/s, respectively. With the exception of the tritium gas load, all parts and materials of the failed specimens have been catalogued and saved.

Further Phase 2 Tests and Results

Since the above failures confirmed and broadened the scope of failures of the Phase 1 series, it was clear that more tests were in order. The Phase 2 series investigates the role of temperature, water content, and surface conditions. We were especially interested in the effect of the prestressing environment (should it be an oxidizing or a reducing atmosphere) on surface conditions.

Fig. 4. Catastrophically failed specimen.

Fig. 5. Edge of failed section (intergranular stress corrosion followed by ductile tearing) (147×).

Table 2. Summary of tritium-loaded stress corrosion failures.

Test phase	Notch	Teflon (g)	Water (ppm)	Yield point gas	Fill pressure (MPa)	Temperature (°C)	Tube serial No.	Test information	Disposition
1	Yes	1.431	500	D_2	137.8	104	0757	Failed by pinhole-type stress corrosion, leak path intergranular corrosion	Specimen cut and held for study, time to failure 11 h 35 min
1	Yes	1.386	500	D_2	110.3	104	0757	Failed by pinhole-type stress corrosion, leak path intergranular corrosion	Scanning electron microscope photos, auger spectroscopy, time to failure 16 h 15 min
1	Yes		500	D_2	137.8	104	0757	Still running	
1	Yes		500	D_2	110.3	104	0757	Still running	
2.1	Yes	1.147	500	D_2	137.8	104	0754	Extensive intergranular stress corrosion, catastrophic failure	Scanning electron microscope photos, time to failure 16 h 12 min
2.1	-	1.339	500	D_2	110.3	104	0754	Ductile dimple failure by intergranular stress corrosion	Scanning electron microscope photos, time to failure 25 h 40 min
2.1	Yes	1.302	500	D_2	82.7	104	0754	Extensive intergranular stress corrosion, catastrophic failure	Scanning electron microscope photos, time to failure 31 h 32 min
2.1	Yes	1.400	500	D_2	82.7	104	0754	Extensive intergranular stress corrosion, catastrophic failure	Scanning electron microscope photos, time to failure 38 h 59 min
2.2	-	1.108		D_2	137.8	104	0762	Still running	
2.2	-	1.168		D_2	68.9	104	0744	Still running	
2.2	-	1.175	500	$He+D_2$	68.9	104	0762	Failed by pinhole-type stress corrosion, leak path intergranular corrosion	Time to failure 35 h 33 min
2.2	-	1.125	500	$He+D_2$	110.3	104	0744	Failed by pinhole-type stress corrosion, leak path intergranular corrosion	Time to failure 22 h 55 min
2.2	-	1.383	500	D_2	110.3	24	0744	Extensive intergranular stress corrosion, catastrophic failure	Time to failure 182 h
2.2	-	1.369	500	$He+D_2$	110.3	24	0744	After failure of F5, the residual gas dropped the temperature to 26 °C Failed by pinhole-type stress corrosion leak path intergranular corrosion	Time to failure 288 h

Table 2 shows the results of the third test series (labeled 2.2). It is now evident that temperature and water content do play a dramatic role. Prestressing the specimens in either oxidizing or reducing atmosphere plays no significant role in preventing the stress corrosion attack. As in the earlier tests, the effect of stress and tritium concentration vs time to failure is linear (Fig. 6).

The third series failed specimens are presently being decontaminated. Metallurgical and surface examination will follow. To date, the failures have been characterized as definitely a severe stress corrosion attack induced by (H,T) F and water. Fluoride compounds have been identified on the cracked surfaces and some indication of depletion of chromium content on the i.d. surfaces is indicated.

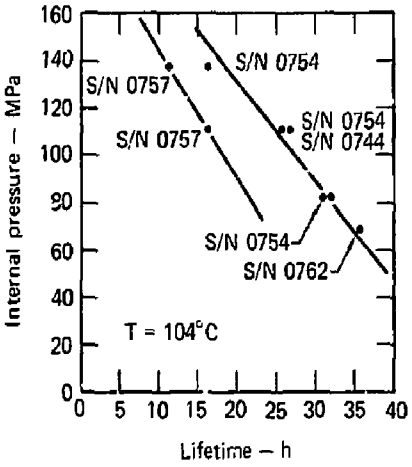

Fig. 6. Internal pressure versus lifetime for tritium gas samples listed in Table 2. S/N refers to tube serial number.

Conclusions

We have found that in the presence of Teflon, tritium, and water, the corrosion of 316 stainless steel is severe. We are continuing our work and will report the results as they are obtained.

An interesting and unintended application for our experimental apparatus has emerged: using it to evaluate stress corrosion theories and the kinetics of stainless steel. This application has met with general enthusiasm; several features make it superior to methods currently available for such applications. These include: everything is self-contained in a small volume, a large amount of water (solvent) is not required, the time of reaction is short and can be controlled, and the tests are relatively inexpensive.

NICKEL-CHROMIUM STRAIN GAGES FOR CRYOGENIC STRESS ANALYSIS OF SUPERCONDUCTING STRUCTURES IN HIGH MAGNETIC FIELDS

Design verification of large superconducting magnets for the LLL Mirror Fusion Test Facility requires measurement of thermal stresses during cooldown and of strains due to magnetic loads at 4.2 K. Strain gages for this and other future large superconducting magnets for fusion research must be able to accurately measure strain in the following applications:

- Tensile tests of superconductors to 10,000 μm/m at 4.2 K and magnetic fields to 12 T.
- Stress analysis on magnets to ± 1000 μm/m during cooldown to 4.2 K without magnetic fields.
- Stress analysis on magnets to ± 3000 μm/m at 4.2 K and magnetic fields to 12 T.

Since published information has been inadequate to make valid and reliable strain measurements for the above applications,[5] we began and are continuing a comprehensive study of the required strain gages. In the first portion of this research, reported in Ref. 6, we found:

- The Micro-Measurements WK-15 strain gage provided the flattest thermal zeroshift (apparent strain) curve between ambient temperature and 4.2 K for Nb_3Sn multifilament conductors, NbTi multifilament conductors, 316 stainless steel, 21-6-9 stainless steel, and OFHC copper when compared with WK-06, WK-09, and WK-13 strain gages.
- We selected as the standard strain gage, the Micro-Measurements WK-15-250BG-350, for all future applications. This is a glass-fiber-reinforced, epoxy-phenolic-resin-backed strain gage with a modified Karma (nickel-chromium) strain sensing foil.
- A special lot of K-15 foil was placed on reserve at Micro-Measurements to provide about 1300 strain gages of the 250BG pattern. We did this to reduce the number of variables that could influence cryogenic strain measurements in high magnetic fields.
- We measured self-heating zeroshifts at 4.2 K for both continuous and pulsed constant current (40 ms on, 10 s off) bridge supplies. Grid-power dissipation was varied from 1 to 1000 mW/cm^2 during the time current was on. We selected a 5-mA (44 mW/cm^2) strain gage current to the 250BG strain gage for all future tests. For this power dissipation, there is no significant difference between zeroshifts for continuous and pulsed constant current.
- The gage factor at 4.2 K was measured to be 5% higher than at ambient for the 250BG strain gage for both tension and compression. This data is an average of four gages in tension and two gages in compression to 1000 μm/m. The spread in gage factor ranged from +4.7 to +5.3%.

We report here on the second part of our research which focused on strain gage magnetoresistance: the change in strain gage resistance produced by a magnetic field. To correct strain gage data for this effect, we measured the magnitude and variation of the magnetoresistance of a large number of strain gages under the following conditions:

- DC magnetic fields to 12 T.
- Three orthogonal field directions.
- Increasing and decreasing fields.
- A wide range of strain levels.
- Liquid-helium temperature, 4.2 K.

Experimental Apparatus to Measure Strain Gage Magnetoresistance

A 6.35-mm-sq bar of ETP copper was cut to a 0.71-m length. We installed eight strain gages at the center of the bar, two on each of the four sides of the bar (Fig. 7). The strain gages were Micro-Measurements WK-15-250BG-350, Lot No. DG-K09FG14, with a 2.15 gage factor at 297 K and a 2.26 gage factor at 4.2 K.

The gages were bonded with M-Bond 600 adhesive and cured 2 h at 366 K. No protective coating was applied over the strain gages. Continuous three-wire leads connected each strain gage to its separate equal-resistance-arm bridge located at ambient temperature. We tested these eight strain gages for magnetoresistance.

Four more strain gages identical to those above were bonded to the copper bar near one end using AE-10 adhesive. These strain gages were not exposed to a significant magnetic field (less than 0.22 T when the magnet was producing 12 T), but were used to monitor the strain in the test bar and its variation during testing.

The test bar was mounted in Deis' cryogenic tensile test apparatus (Fig. 8).[7] A load cell at ambient temperature monitored the force on the copper bar. We used the tensile test apparatus in the load-control mode during testing.

A superconducting magnet with a field strength up to 12 T (Fig. 8) was centered over the eight strain

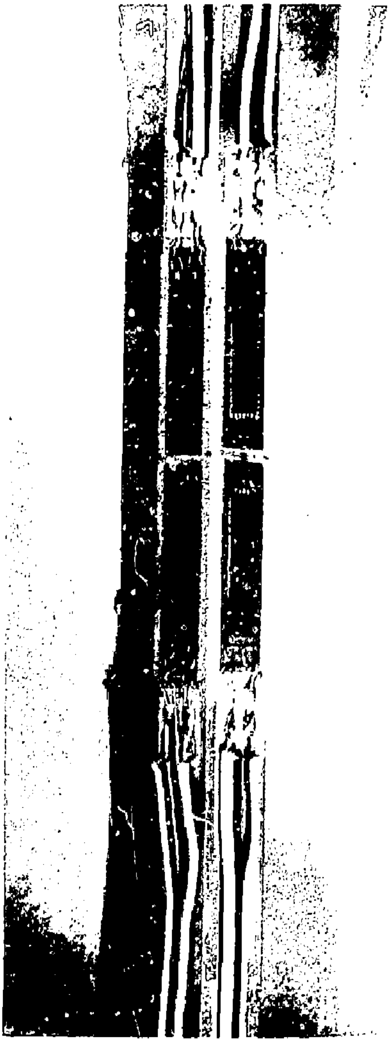

Fig. 7. [illegible] magnetoresistance test gages bonded to ETP copper test bar (WK-15-250BG-350 strain gages).

[illegible] of the copper test bar. The [illegible] to the grid-plane of four [illegible] direction 1 in Fig. 9). For the [illegible] the magnetic field was [illegible] plane and perpendicular to the [illegible] of the strain gages (direction 2 [illegible] Fig. 9). The magnetic field was about the same [illegible] gage locations.

[illegible] enclosed the superconducting magnet [illegible] length of the copper test bar including [illegible] each end. For all tests, the entire copper [illegible] immersed in liquid helium (4.2 K).

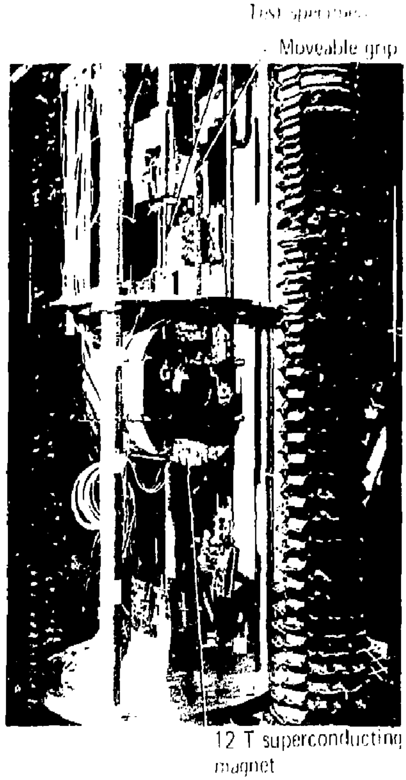

Fig. 8. Tensile test apparatus showing superconducting magnet centered over magnetoresistance test gages on ETP copper test bar.

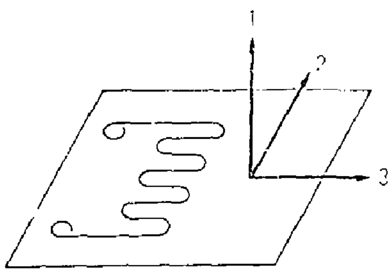

Fig. 9. Magnetic field directions relative to strain gage geometry.

We measured the strain gage [illegible] with a computer controlled data acquisition system. This system powered the channels sequentially with pulsed constant current. It measured the output voltage with an integrating digital voltmeter without amplification at the rate of 10 channels/s. We used a standard strain gage current of [illegible] mA

Table 3. Results of magnetoresistance tests.

Strain level (μm/m)	200		900		2900		8900		6300
Strain-gage No.	5-8	1-4	5-8	1-4	5-8	1-4	5-8	1-4	1-8
Field direction	1	2	1	2	1	2	1	2	3
DC magnetic field (T)	Strain error[a] (μm/m)								
0	0	0	–	–	–	–	–	–	0
0.35	–	–	−6(2,−1)	−6(2,−3)	–	–	–	–	−10(2,−2)
0.43	–	–	–	–	−6(1,−1)	−6(3,−3)	–	–	−10(2,−2)
0.5	–	–	–	–	–	–	−6(2,−1)	−4(2,−4)	−10(2,−2)
1	−9(1,−1)	−8(2,−4)	−9(1,−1)[b]	−8(2,−4)[b]	−9(1,−1)[b]	−8(2,−4)[b]	−9(1,−1)[b]	−8(2,−4)[b]	−8(2,−4)
2	7(0,−1)	8(2,−4)	5(1,−1)	5(3,−4)	5(1,−1)	5(3,−4)	3(1,−1)	3(2,−4)	8(2,−3)
3	33(1,−1)	34(3,−4)	31(1,−1)	32(3,−5)	–	–	–	–	36(2,−4)
4	70(1,0)	71(3,−4)	67(1,−1)	67(4,−5)	66(1,−1)	67(3,−5)	63(1,0)	63(3,−4)	72(2,−4)
5	108(1,0)	109(3,−4)	105(1,−1)	105(4,−5)	–	–	–	–	108(4,−3)
6	150(1,−1)	151(3,−4)	148(1,−1)	149(4,−6)	147(1,0)	148(3,−5)	144(1,−1)	144(3,−5)	151(3,−4)
7	192(1,0)	193(4,−5)	191(1,−1)	192(4,−7)	–		–	–	192(3,−5)
8	235(1,−1)	236(4,−5)	234(1,−1)	234(5,−6)	–		–	–	235(3,−6)
9	278(1,−1)	279(3,−6)	276(1,−1)	277(4,−6)	274(1,−1)	274(3,−5)	271(1,−3)	270(4,−5)	277(3,−6)
10	319(1,−1)	320(3,−5)	319(1,−1)	319(5,−6)	–	–	–	–	318(4,−7)
11	360(1,−1)	363(2,−1)	359(1,−1)	360(5,−7)	–		–	–	358(5,−7)
12	400(2,−1)	402(4,−6)	401(1,−1)	402(6,−7)	398(2,−1)	398(4,−4)	393(2,−3)	393(4,−5)	397(5,−7)
11	359(1,−1)	359(4,−6)	358(1,−1)	359(5,−8)				–	356(7,−8)
10	316(1,−1)	318(3,−6)	316(2,−1)	318(5,−8)	–			–	314(7,−9)
9	272(1,0)	274(4,−6)	273(1,−1)	275(7,−8)	272(1,−1)	272(3,−5)	266(1,−2)	265(4,−4)	272(6,−8)
8	229(0,−1)	230(4,−6)	229(1,−1)	231(6,−8)		–	–	–	228(7,−9)
7	186(0,−1)	187(4,−6)	185(1,−1)	187(5,−8)	–	–			186(7,−9)
6	143(1,−1)	144(4,−6)	144(1,−1)	146(6,−8)	142(1,−1)	142(3,−4)	138(1,−2)	137(4,−3)	144(8,−10)
5	99(1,−1)	102(3,−6)	101(1,−1)	103(6,−8)	–	–	–		101(9,−10)
4	62(0,−1)	64(3,−5)	63(1,−1)	65(5,−8)	61(1,−1)	62(2,−4)	58(1,−2)	56(4,−2)	62(6,−9)
3	25(0,−1)	27(3,−5)	27(1,−2)	29(6,−8)	–	–	–	–	27(9,−9)
2	3(4,−3)	3(2,−5)	1(1,−2)	4(5,−8)	2(1,−1)	3(2,−4)	0(1,−1)	−1(3,−2)	0(10,−9)
1	−12(1,−1)	−9(3,−4)	−11(1,−1)	−9(6,7)	−10(2,−1)	−10(3,−2)	−9(2,−1)	−10(3,−1)	−13(10,−7)
0.5	–	–	–	–	−7(1,−1)	−7(2,−2)	–	–	–
0.43	–	–	−7(1,−2)	−5(5,−7)	–	–	−5(2,−2)	−6(2,−2)	–
0.35	−8(1,−1)	−5(3,−5)	–	–	–	–	–	–	−10(11,−7)

[a]Maximum variation in parenthesis.

[b]Data from 200-μm/m run.

The data from the 1-kHz sinusoidal carrier excitation strain indicator and the pulsed constant current measuring system were in all cases identical, within the 2.5-μm/m resolution of the strain indicator. There was no evidence that spurious voltages were present anywhere in the strain gage circuits.

Discussion

From Fig. 10, it appears that the magnetoresistance for the eight strain gages at 4.2 K is independent of

- magnetic field direction,
- increasing or decreasing field (hysteresis), and
- tension strain levels ranging from 200 to 8900 μm/m.

The maximum variation in magnetoresistance for eight strain gages, three magnetic field directions, five tension strain levels, and increasing and decreasing field strength was about ±10 μm/m at any value of magnetic field. This result is negligibly small and well within the acceptable variation for practical strain measurements for stress analysis. The magnetoresistance is essentially linear with magnetic field from 4 to 12 T.

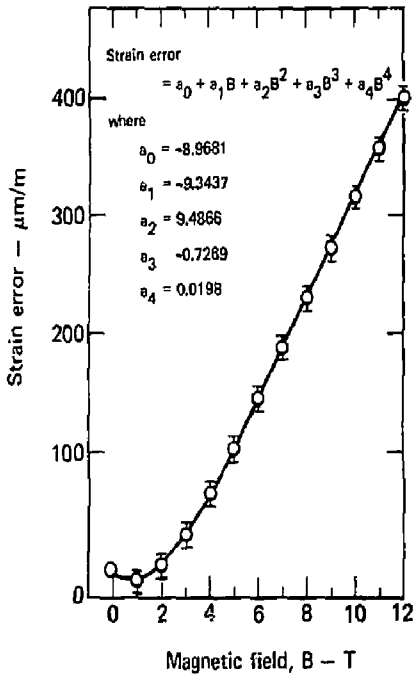

Fig. 10. Magnetoresistance strain error calibration curve as function of magnetic field at 4.2 K (WK-15-250BG-350 strain gages). Summary of data for eight strain gages, three field directions, strain levels of 200, 900, 2900, 8900, and 6300 μm/m, and increasing and decreasing fields.

The data in Fig. 10 are similar to data reported by Greenough[8] to 2.5 T, Walstrom[9] to 6 T, and Hartwig[10] to 7 T for Micro-Measurements modified Karma alloy strain gages at 4.2 K.

For at least one strain gage, type WK-15-250BG-350, Walstrom[9] observed an increase in magnetoresistance of about 13 μm/m per 1000 μm/m of nominal strain on an aluminum test beam from 3 to 6 T. We did not observe any such strain dependence of magnetoresistance for strain levels from 200 to 8900 μm/m.

Greenough[8] observed an anomaly in the magnetoresistance for two SK-09-031DE-350 strain gages from the same lot number, both of which were tested in fields to 2.5 T and with fields perpendicular and parallel to the gage. The magnetoresistance for one gage followed the characteristic curve expected for Karma alloy gages. The other gage of the same lot number exhibited nearly zero magnetoresistance at fields to 2.5 T. We have not observed such an anomaly either in the eight WK-15-250BG-350 strain gages reported here or in preliminary magnetoresistance measurements performed on four WK-15-125AD-350 strain gages.

Although we have not measured the magnetoresistance of strain gages in compression, we would expect the same results as in Fig. 10. It seems logical that if the magnetoresistance is strain-level independent from +200 to +8900 μm/m, then this independence should hold true for compression strains.

Conclusion

We measured the magnetoresistance for eight of our standard strain gages (WK-15-250BG-350, Lot No. DG-K09FG14) for magnetic fields to 12 T at 4.2 K. The magnetoresistance data were essentially independent of field direction, increasing or decreasing field, and tension strain levels from 200 to 8900 μm/m. The data were essentially a unique function with magnetic field and were least-squares-curve-fit by a polynomial equation. The variation in magnetoresistance data was typically ±10 μm/m, which is negligibly small for practical stress analysis. This magnetoresistance calibration curve will enable us to correct measured data for magnetic field effects.

We have already successfully used these strain gages to measure superconductor mechanical properties. We will soon use the gages in the stress analysis of superconducting fusion magnets during cooldown from ambient temperatures and during operation at 4.2 K with magnetic fields to 12 T.

VARIABILITIES DETECTED BY ACOUSTIC EMISSION FROM FILAMENT-WOUND ARAMID FIBER/EPOXY COMPOSITE PRESSURE VESSELS

For several years we have been studying the acoustic emission technique as a means of examining filament-wound aramid fiber/epoxy composite structures. Such structures are being used with increasing frequency in applications where a high strength-to-weight ratio is required, such as for pressure vessels on the Space Shuttle[11] and for the rocket motor case on the Trident missile.[12] Our previous work included studies on the application of acoustic emission to the prediction of the burst pressure of composite pressure vessels.[13,14]

We chose the acoustic emission (AE) technique as the most promising inspection technique for solving the nondestructive testing problems unique to fiber

composite vessels. There are two inspections that must be made after the composite structure is fabricated. First, an inspection of the macroscopically distributed material must be made to check fabrication process control. For example, does the fiber-to-matrix interfacial bond have the required strength? Are the fiber and epoxy contents correct? Is the void content sufficiently small? Second, an inspection must be made for local defects that will render the structure unable to function under the design conditions. The net result is that the nondestructive testing problem for a fiber/epoxy composite structure is usually much more extensive than that for a completed metal structure. Furthermore, it is not normally possible to "cut off" a piece of the composite material and conduct destructive strength or microscopic examinations of the material, so some of the approaches that are applicable to metals are not suitable for filament-wound composites.

The AE technique offers the possibility of performing both the required inspections because it is sensitive to macro- and microfailure events occurring throughout the pressurized fiber composite vessel. Thus, by dividing the AE data up into two classes, we can use the AE that is generated essentially uniformly throughout the composite to make statements about the general material properties of the fiber composite. We also can use the AE data that is generated at various specific positions in the composite to assess the severity of local defects in the composite structure. The first class of data tends to consist of more numerous AE events of lower amplitude. The second class of data, because it results from growing local defects, tends to consist of fewer AE events of higher amplitude, occurring at higher stresses.

In this article, we report on the AE data gathered during proof tests of a random set of 30 spherical Kevlar/epoxy pressure vessels taken from a production total of 250 vessels. These data then are examined to determine the usefulness of AE for the inspections we believe necessary for such fiber composite structures. Particular emphasis is placed on the vessel-to-vessel changes in the first class of AE data and on the possible use of this AE for identifying the significant production process-control problems in the manufacture of fiber composites.

Materials and Filament Winding

The organic fiber Kevlar 49 (DuPont, 380 denier) was used with the epoxy system DER 322 (Dow Chemical)/Jeffamine T-403 (Jefferson Chemical) in a 100/44.7 ratio. The composite was filament-wound into 114-mm-diameter spherical pressure vessels over 1100 aluminum (1.02-mm wall thickness) spherical mandrels (Fig. 11). Before winding, the mandrel was prepared by first cleaning with methylethyl ketone and acetone and then vapor-degreasing with trichloroethylene. A coating of adhesive (3 g of XD 7575.02/DER 332/ETOH amine in a 40/10/6 ratio) was placed between the aluminum and the composite. The adhesive was gelled at room temperature for 24 to 72 h before filament-winding was begun. The wall thickness of the composite was about 1.1 mm and the average burst pressure of the metal-lined composite pressure vessel, based on burst tests of 30 vessels, was 34.5 MPa. See Fig. 12 for a photograph of a typical vessel.

The filament-winding was done on an LLI, designed and built, computer-controlled spherical winder. Details of this four-axis, fully programmable sphere-winding machine are given in Ref. 15. Winding of a wide-band, multiangle pattern starts at the waist and proceeds to the bosses. The single-end fiber was impregnated with epoxy and wound at a tension of 2.3 N. Complete data on winding and vessel parameters were obtained during the winding and curing process.

Testing and Results

The proof tests were conducted using water mixed with soluble oil (about 40 parts water to 1 part soluble oil) to pressurize the vessels at a constant rate of 1.15×10^{-1} MPa/s using a feedback control system. Each vessel was pressurized to 25.39 ± 0.15 MPa, 74% of the expected failure pressure. The peak pressure was held for 1 min, after which the pressure was reduced to zero in about 1 min. All tests were in a controlled-temperature room at room temperature (21 ± 3°C). Two channels of AE data were gathered. Figure 12 shows the fixture used and the positions of the two transducers (transducers were separated by 120 deg on the vessel waist); Fig. 13 shows the AE test system components. The AE transducers were Dunegan/Endevco S-140A resonant-type, modified by machining away part of the epoxy shoe.[14] The AE system, test fixture, and *in situ* calibration technique also have been described in detail in Ref. 14. Briefly, the vessel first was pressurized to 2.1 MPa in the fixture. Then, the gain was adjusted in each channel so that the average peak output of the Hewlett-Packard 3400A root-mean-square (rms) meters was between 580 and 620 mV for four consecutive pencil lead fractures (0.3 mm in diameter by 4 mm long, Pentel 2H) against the vessel (see Fig. 12). An oscilloscope photograph of the time domain was taken with the AE system transient recorder for a

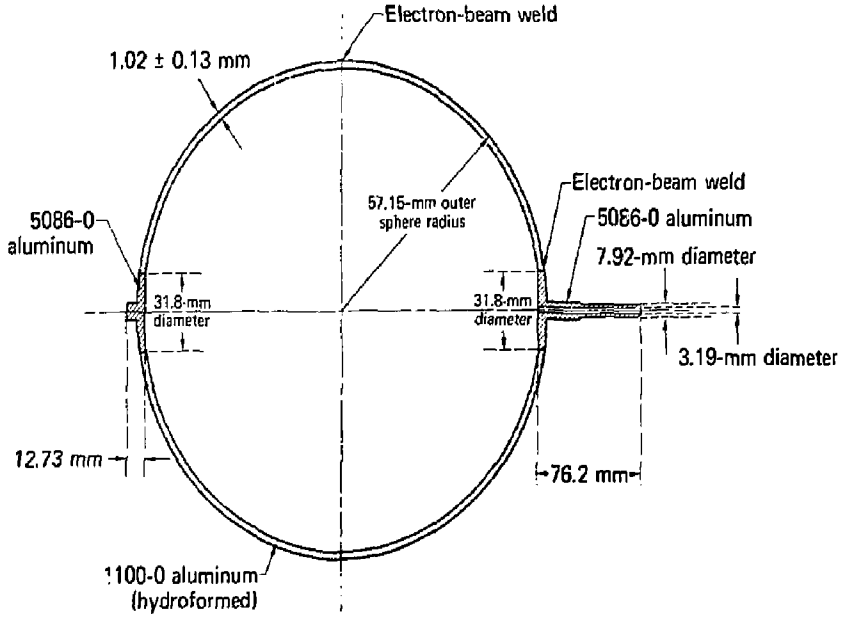

Fig. 11. Design of the aluminum mandrel.

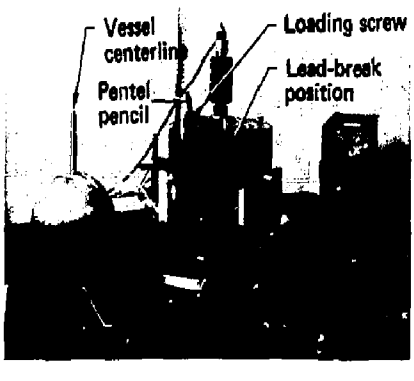

Fig. 12. Typical spherical Kevlar 49/epoxy composite pressure vessel on cork donut and another vessel mounted in the calibration-monitoring fixture.

calibrating lead fracture for each vessel. Photographs are given in Fig. 14, showing the typical repeatability of this calibration approach.

The actual proof tests were run by increasing the calibration gain in channel 1 by 8 dB and by decreasing the calibration gain in channel 2 by 2 dB. The total AE system gains were too low to be sensitive to any AE generated by events in the metal liner. Figure 15 shows some typical time and frequency domains of AE events which were obtained using the AE system transient recorder and spectrum analyzer. As observed in Ref. 14, both local (Fig. 15b) and global (Fig. 15a,c) AE burst events occurred. Data on the rms dc output vs time (from strip chart recorders) during the proof tests are given in Fig. 16. The peaks of the spikes on these plots are related to the total energy out of the transducer for the AE bursts. The relatively continuous dc level is related to the total energy out of the AE transducer for the numerous smaller amplitude AE bursts which approach quasi-continuous AE over certain pressure ranges. The three tests shown in Fig. 16 are representative of the extremes in the AE data obtained from the proof tests.

Discussion

The general character of the AE generated during these proof tests shows two significant aspects (see Fig. 16). First, the dc output of the rms meters has a more or less quasi-continuous level that changes rather slowly with time. Second, superimposed on the continuous level are "spikes" in the rms data that are caused by relatively large amplitude AE events. Because of the dual character of the AE obtained from such fiber composite vessel proof tests, it is clearly advantageous to use two separate AE gains. The higher gain data is useful for determining

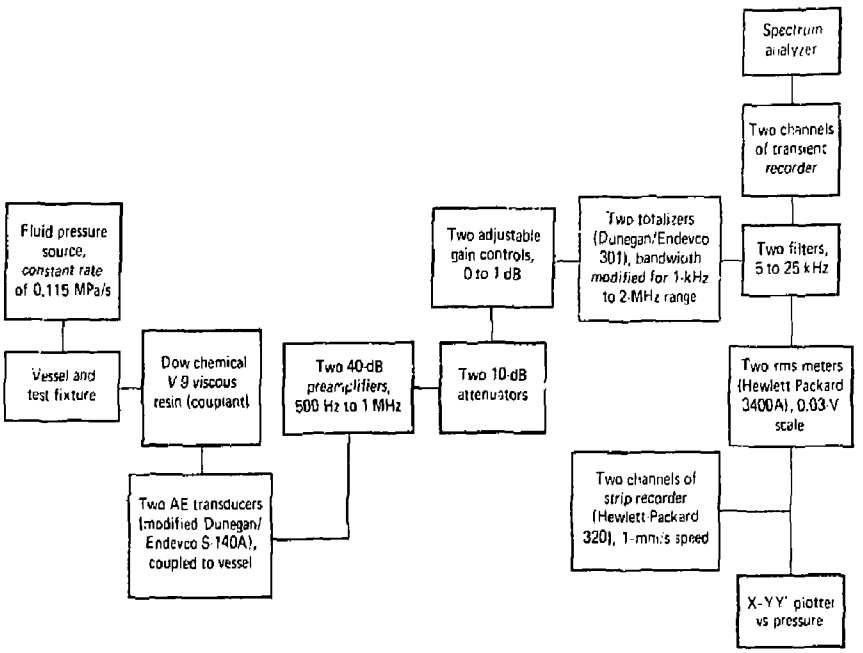

Fig. 13. Diagram of the AE test system components.

the quasi-continuous level of AE whereas the lower gain data enables us to determine the approximate energy of the large AE bursts.

With this approach, we can inspect two aspects of the fiber composite structure. We believe the lower amplitude, more numerous AE events that result in the quasi-continuous AE represent numerous microfailure events that are occurring throughout the composite. This type of failure mechanism explains the early peak in the continuous level of AE, occurring between 32 and 36% of the expected failure pressure. From the work of Ref. 16, we believe that this early peak is caused by AE which is generated by cracks occurring parallel to the direction of the bands of parallel fibers which make up the filament-winding pattern. This cracking of the matrix that causes filament failures results from local stresses perpendicular to the band direction, which occur in the biaxially loaded composite pressure vessel. As this cracking progresses, the uncracked portions of the composite are exhausted and thus this failure mechanism gradually decays away.

The larger amplitude (i.e., greater energy) AE bursts are much fewer in number and represent AE events that occur at local locations of high stress or flawed composite. In our opinion, these events are closely related to the growth of defects in the composite which ultimately determines the burst strength of the vessel. In most cases, the source event is probably the almost simultaneous failure of several fibers at a particular location. These large events probably are occurring at several locations throughout the composite. Thus, to predict burst pressures, it will be necessary to categorize the large AE bursts according to their source location. However, because of the nonhomogenous nature of the filament-wound composite, it may be difficult to use the same successful techniques of source location in a composite pressure vessel as are used in metal pressure vessels. Thus, an alternative technique may have to be developed so we can recognize large AE events originating from the same location.

It is clear from Fig. 16 that there are significant differences in the AE signature or pattern generated during the proof tests. This implies that some parameter in the manufacturing process has changed, causing the resulting composite vessels to exhibit significantly different microfailure events and/or failure mechanisms. The change in the level of the relatively continuous rms dc output that peaks early in the proof test is of particular interest.

Because this peak is the result of numerous AE bursts of relatively small amplitude that occur throughout the vessel, we assume that the changes in level of this peak represent significant changes in the state of the manufactured composite material.

We have monitored numerous parameters during the filament-winding process but, to date, have not been able to determine what parameters in the manufacturing process are causing the AE changes. The reasons for this result may be included among the following. First, a number of variables change from vessel to vessel but the changes are neither consistent nor predictable. Second, there may be possible interactions between the variables. In addition, limited physical inspection of the outer surface of the composite vessels has not revealed any positive correlation between visible surface damage and the changes in the AE generated during the proof test. In future research, we plan to follow two approaches in an attempt to determine the causes of the AE changes. Vessels will be manufactured with deliberate extreme changes in certain parameters. Also, we will destructively inspect the microstructure of vessels that are identified by AE from a proof test as significantly different.

During burst tests of vessels taken from the set of 250 vessels, we observed that the burst pressures did not correlate with the different AE patterns generated during the proof tests. Because the current set of vessels is being tested in stress-rupture to failure at 74% of their expected burst pressure, we may find a correlation between lifetime and the AE pattern determined during the proof tests. These results will be published when these long-term stress-rupture tests are completed. Perhaps the vessels exhibiting the greatest AE activity during the proof test will have the shortest lifetime; the AE indicates that these vessels suffered more damage and have more damage sites which may result in a more rapid degradation of these vessels.

With this hypothesis in mind, we have made several rankings of the vessels by expected order of failure in the stress-rupture testing. However, because of leaking vessels, difficulties in the AE system, or lack of differences between vessels, we were not able to include all vessels in the various rankings. In Table 4, the vessels are ranked first according to the amplitude of the peak of the relatively continuous dc output from the rms meter. The rms data obtained from channel 1 (higher gain) were used for this ranking. The rest of the rankings were made with data taken from channel 2 (lower gain). The total number of burst events with a dc output greater than 50 mV as well as the pressure at

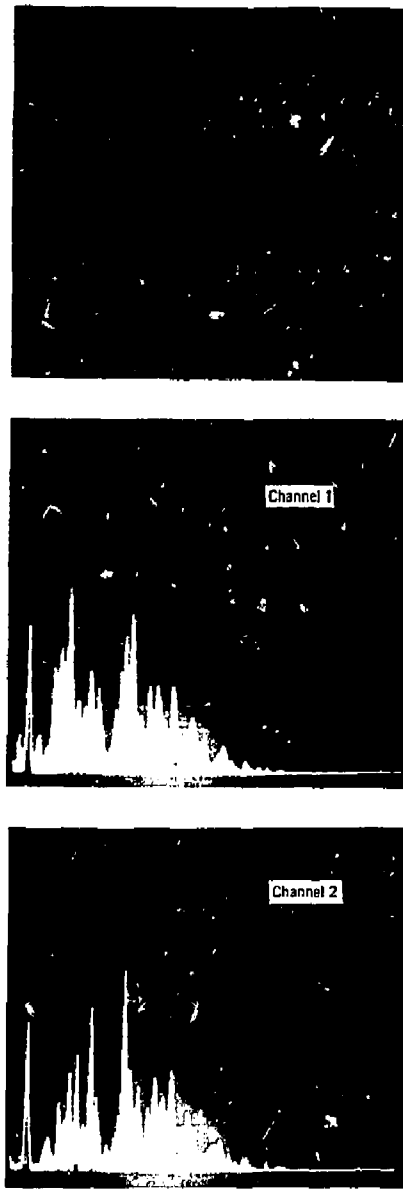

Fig. 14. Time and frequency domains for calibration pencil lead breaks on composite pressure vessel No. 243. Scale divisions are, vertically, 0.4 V/cm (time) and 50 mV/cm (frequency) and, horizontally, 0.4 ms/cm (time) and 5 kHz/cm (frequency). The calibration pressure was 2.1 MPa. In the top photo, the upper time tracing is taken from channel 1, the lower time tracing from channel 2.

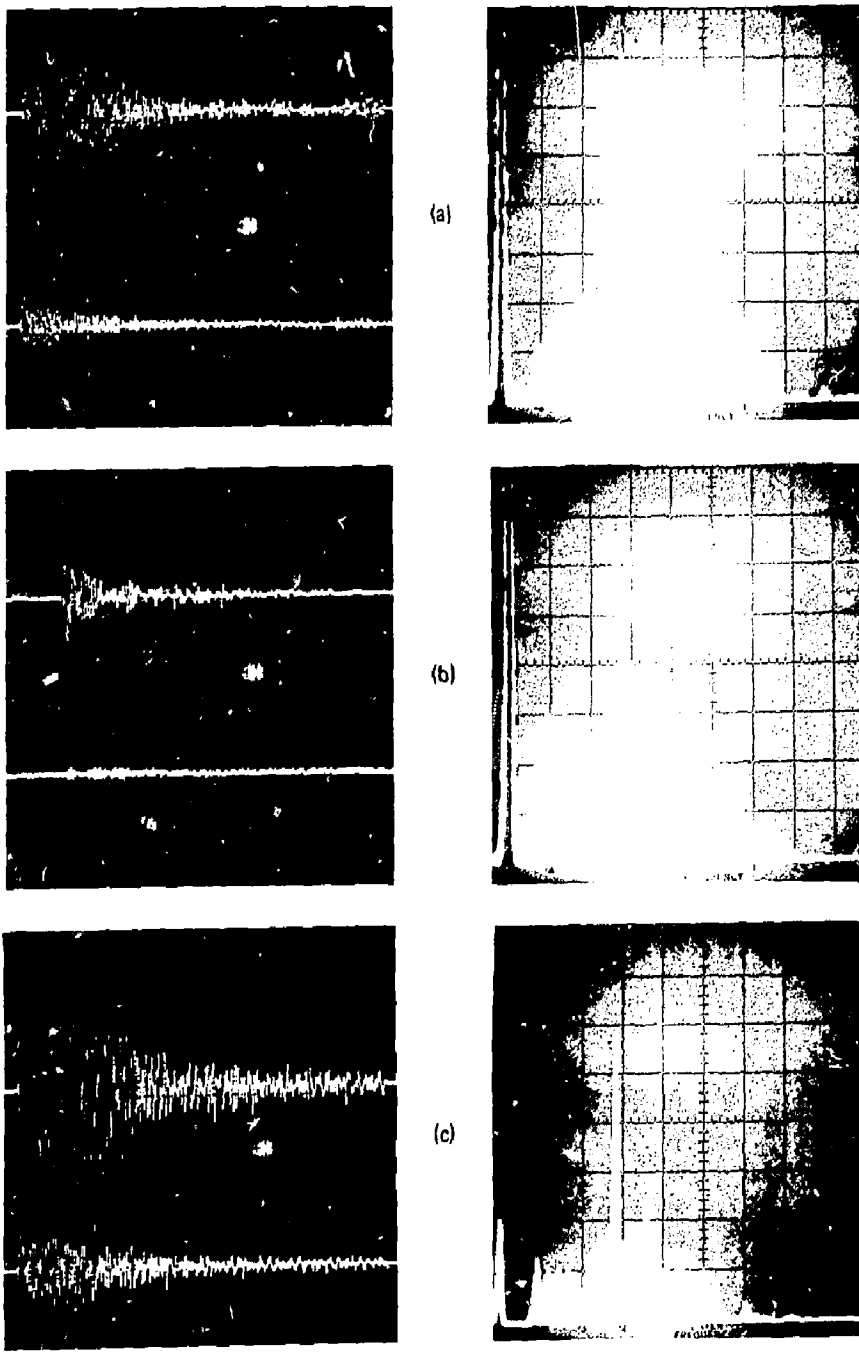

Fig. 15. Time and frequency domains for typical AE bursts during proof testing. Scale divisions are, vertically, 0.2 V/cm (a,b) and 1.0 V/cm (c) for time domains and arbitrary linear divisions for frequency domains. Horizontally, scale divisions are 1 ms/cm (time) and 5 kHz/cm (frequency), starting at zero. The upper time sweeps are taken from channel 1, the lower time sweeps are taken from channel 2; there is a 10-dB difference in gain between the two channels. Approximate vessels pressures were 14.5, 16.6, and 26.2 MPa for (a), (b), and (c), respectively.

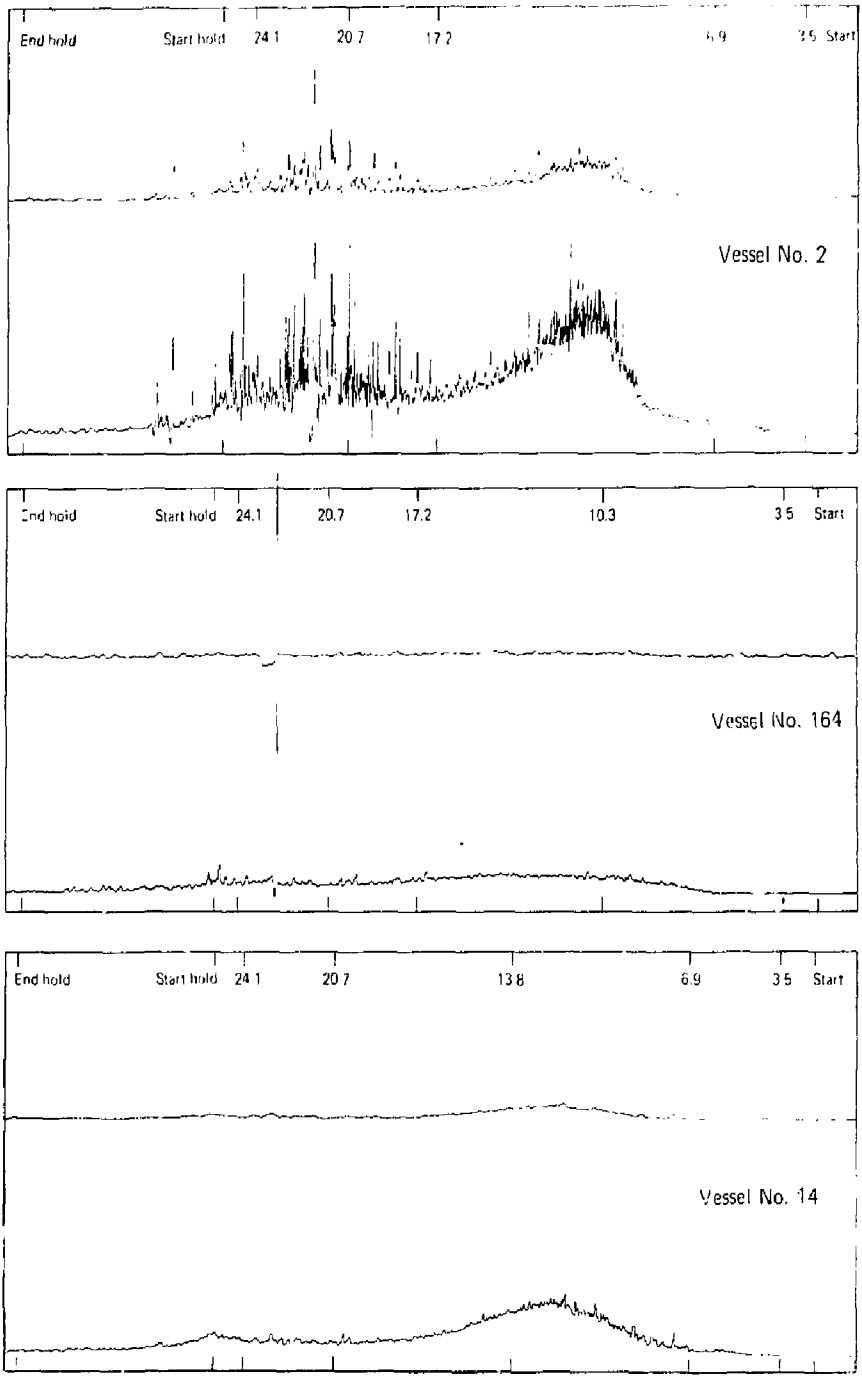

Fig. 16. Strip chart plots of rms meter dc output vs time for proof tests of three vessels (pressure in MPa given at top of strips). There is a 10-dB difference in gain between channel 1 (lower tracings) and channel 2 (upper tracings).

Table 4. Various rankings of composite pressure vessels according to AE-monitored damage generated during the proof tests (greatest amount of damage ranked first).

Height of first peak		Burst energy during 1-min hold		Number of burst events during proof test		Total burst energy during proof test		Pressure for first burst >600 mV dc output	
Vessel number	Major divisions	Vessel number	Arbitrary energy units	Vessel number	No. events >50 mV dc output	Vessel number	Arbitrary energy units	Vessel number	MPa
2	6.0	248	15.0	2	27	248	77.4	236	12.1
50	5.4	50	11.1	50	25	50	76.4	174	14.4
236	5.1	2	2.4	114	21	70	70.4	50	19.5
231	4.9	114	0.5	56	19	236	70.4	70	20.9
25	4.9	—[a]		248	18	2	66.6	103	21.5
45	4.6			25	14	174	34.7	2	21.8
248	4.7			70	13	164	33.1	164	22.6
92	4.6			123	10	25	30.2	248	25.2
153	4.4			93	8	114	22.0	—[b]	
240	4.1			236	7	56	21.2		
234	4.1			35	5	103	17.4		
56	4.0			240	4	123	10.4		
174	3.9			174	4	93	8.9		
93	3.7			45	3	35	2.6		
39	3.7			103	2	45	2.2		
112	3.6			153	2	234	1.7		
114	3.5			234	2	240	1.6		
35	3.4			112	1	153	0.9		
14	2.7			39	1	39	0.7		
103	2.7			184	1	112	0.4		
70	2.6			164	1	184	0.4		
184	2.2			14	0	14	0		
164	0.9								

[a] No bursts during the 1-min hold for the remainder of the pressure vessels.

[b] No bursts >600 mV during the proof test for the remainder of the pressure vessels.

which the first AE burst with a dc output greater than 600 mV occurred also were used to rank vessels. Finally, two energy type rankings were made. The energy out of the AE transducer per AE burst on an arbitrary scale was calculated from the equations developed in Ref. 14. The vessels were ranked according to total energy during the proof test.

Four important practical applications of AE to fiber composites are apparent from the above results. First, AE techniques can be used to identify a composite manufacturing process change that causes significantly different microfailure conditions to occur when the composite is stressed. Also, AE methods can be used to single out those composite vessels which exhibit extremes in microfailure processes. These vessels then can be destructively inspected to determine the differences in source mechanism. Third, once the parameters that control the vessel variations are identified, AE can easily determine the production operating limits required to produce composite vessels with consistent AE signatures. Lastly, once the out-of-control parameters have been brought within the necessary limits, the AE test can be used to determine whether or not the composite vessel was fabricated properly.

There are several important engineering consequences of the unknown cause of variations in the composite pressure vessels. Mechanical properties such as strength, lifetime, and creep that are determined in composite vessels with one characteristic AE pattern may not be the same for vessels with a significantly different AE pattern. Thus, part of a production lot might not meet the lifetime performance requirements. In addition, it is difficult to develop a technique to predict burst pressures when

process variations cause significant changes in the AE patterns but do not significantly change the burst pressure. Finally, confidence in the long-term structural reliability of such composite vessels is decreased because the fabrication process does not seem to be closely controlled.

Conclusions

From these proof tests, we draw four principal conclusions. First, the AE data indicate that the amount of damage done during a proof test to supposedly identical, filament-wound Kevlar/epoxy vessels varies significantly. Second, differences in proof-test-generated AE raises questions about the consistency of mechanical properties of filament-wound Kevlar/epoxy pressure vessels. Also, because of the unexplained variations in AE that are not related to burst pressure, it is difficult to predict burst pressures from the AE data. Lastly, AE can be used to identify vessels with extreme differences in AE proof pattern; these then can be destructively inspected to determine differences in microscopic damage.

ON-LINE MODAL ANALYSIS USING THE T-DAC COMPUTER SYSTEM

Introduction

An understanding of the vibration modes of a structure is needed to predict how it will respond to any dynamic loading. This can be obtained by modal analysis, the process of experimentally determining the vibration natural frequencies, mode shapes, and damping coefficients of a mechanical structure. These modal parameters can then be used by simulation codes to predict the response of a structure to an arbitrary forcing function. Modal analysis software has been written and installed on the T-DAC [17] (*T*ransportable-*D*ata *A*cquisition and *C*ontrol) computer system and has been used to analyze the vibration modes of several structures including the one-fifth-scale pressure suppression experiment torus [18] and the Shiva target frame. Work is under way to enhance the modal analysis capability of the T-DAC system and to link the modal analysis results to existing simulation codes. Experience has shown that this on-line capability is a fast and accurate tool for vibration analysis of structures.

The T-DAC computer system provides an integrated data-acquisition and data-reduction capability that facilitates the rapid modal analysis of complex mechanical structures. A structure's modes of vibration are determined from data obtained by exciting the structure with an impacting device (such as a hammer) and simultaneously measuring the vibration response. A set of input and response measurements is used to compute point-to-point transfer functions (or frequency-response functions) from which all mode shapes, natural frequencies, and damping coefficients within the measurement bandwidth are determined. The computed mode shapes are then illustrated on a CRT screen by displaying an animated three-dimensional line drawing of the structure being analyzed. Figure 17 shows a sample display of a hemi-shell as it appears on the screen. The display oscillates on the screen in the same manner as the actual vibration mode. To assist in interpretation of the data, the operator may rotate the display about any of three mutually perpendicular axes.

This article describes the basic modal analysis capabilities of the T-DAC system and surveys two recent applications.

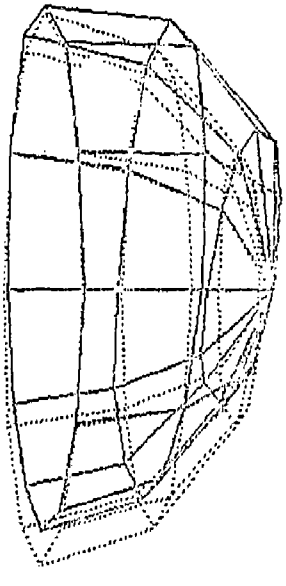

Fig. 17. A three-dimensional modal display of a hemi-shell as it appears on the T-DAC CRT graphics terminal.

Modal Analysis

Although modal analysis is primarily an experimental technique, it is essential to first construct a conceptual mathematical model of the structure to be analyzed. The model is used to select impact locations on the structure and to aid in the interpretation of the results. If the structure cannot be described by a model of the proper form, then the analysis cannot be applied with confidence. Modal analysis can be applied to any system that can be described by a set of simultaneous second-order linear differential equations of the form

$$M\ddot{x}(t) + C\dot{x}(t) + kx(t) = f(t), \qquad (1)$$

where f(t) is the force vector, x(t) is the displacement vector, $\dot{x}(t)$ is the velocity vector, $\ddot{x}(t)$ is the acceleration vector, and M, C, and K are the mass, damping, and stiffness matrices. If the system has n degrees of freedom, then the vectors are n-dimensional and the matrices are n × n. Solutions of the homogeneous equation describe the n different modes of vibration of the system. Results of a modal analysis can be used to compute the M, C, and K matrices from experimental data. Once these matrices are known, it is possible to calculate the response of the system to any arbitrary driving force vector using Eq. (1).

It is necessary to review the theory to illustrate how impact locations are determined and how the mode shapes can be computed. First we will briefly describe some properties of the solutions of the homogeneous form of Eq. (1). Taking the Laplace transform of Eq. (1) gives:

$$B(s)X(s) = F(s), \qquad (2)$$

where F(s) is the Laplace transform of the force vector, X(s) is the Laplace transform of the displacement vector, B(s) equals $Ms^2 + Cs + K$, which is the system matrix, and s is the Laplace variable. The transfer matrix is defined as the inverse of the system matrix

$$H(s) = B(s)^{-1} \qquad (3)$$

which implies that

$$X(s) = H(s)F(s), \qquad (4)$$

Therefore, the transfer matrix is n × n.

$$H(s) = \begin{bmatrix} h_{11}(s) \ldots\ldots h_{1n}(s) \\ \cdot \\ \cdot \\ \cdot \\ h_{n1}(s) \ldots\ldots h_{nn}(s) \end{bmatrix} \qquad (5)$$

where $h_{ij}(s)$ is the transfer function that specifies the response of the *ith* element due to the force applied at the *jth* element. Since the elements of B(s) are quadratic functions of the Laplace variable s, the elements of H(s) are ratios of polynomials in s; i.e.,

$$h_{ij}(s) = \frac{b_0 + b_1 s + \ldots + b_{2n} s^{2n}}{\det(B(s))}, \qquad (6)$$

where the b's are polynomial coefficients and det (B(s)) is a polynomial of order 2n. If the roots of det (B(s)) are distinct, then H(s) can be written as

$$H(s) = \sum_{k=1}^{2n} \frac{a_k}{s - p_k}, \qquad (7)$$

where a_k equals the residue matrix for the k*th* root, and p_k equals the k*th* root of det (B(s)) or k*th* pole of H(s). If the system is subcritically damped, the roots occur in complex conjugate pairs of complex numbers.

$$p_k = -\sigma_k + i\omega_k, \; p_k^* = -\sigma_k - i\omega_k, \qquad (8)$$

where σ_k is the damping coefficient and ω_k is the natural frequency. For each pole there is a corresponding modal vector u_k which is a solution of the equation,

$$B(p_k)u_k = 0 \qquad (9)$$

Using the modal vectors, one can write the transfer matrix in terms of the n complex conjugate pairs of poles

$$H(s) = \sum_{k=1}^{n} \frac{u_k u_k^t}{s - p_k} + \frac{u_k^* u_k^{*t}}{s - p_k^*} \qquad (10)$$

Each term in the summation is an n × n complex matrix that corresponds to the contribution of each mode to the transfer matrix.

It can be shown [19-22] that using Eq. (10) each row and column of the residue matrix contains the same modal vector multiplied by a component of itself. Therefore, the modal vectors and pole locations can be computed from any row or column of the transfer matrix. This means that a structure can be analyzed by exciting it at each point and measuring the response at one point, identifying a column, or by exciting it at one point and measuring the response at every point, identifying a row.

When the modal vectors are real-valued, then they are equivalent to the mode shape. In the case of complex modal vectors, the mode shape can be computed from the magnitude of the residue.

T-DAC

The T-DAC computer system is a powerful data-acquisition tool. Modal analysis data are acquired using the LLL-designed 16-channel transient capture, and the data are then stored on magnetic tape before the data-reduction procedure begins. The modal analysis data-reduction software is a subset of the GPDAP (General Purpose Data Analysis and Plotting) code [22] which runs on the T-DAC system.

Currently, the mode shape software algorithm is simply the straightforward extraction of the imaginary part of the transfer function at a modal frequency selected interactively by the operator. Although this is an adequate algorithm for lightly damped structures with well-separated modes, other algorithms are being developed for use on structures with high damping or high modal density.

The modal display software is capable of driving an animated display of 96 connected nodes based on modal data computed from 48 input/response transfer functions.

One-Fifth-Scale Pressure Suppression Experiment Torus

A modal analysis of the one-fifth-scale torus used in the Nuclear Regulatory Commission's pressure suppression experiment was conducted to determine its fundamental modes of vibration. This knowledge was later used as an aid in the interpretation of the torus test data. It allowed analyzers to identify structural modes present in the data. The conceptual mathematical model (a seven-element lumped mass beam) was used to select appropriate locations for the application of low-level impulsive loads.

The torus was subjected to two series of impacts, vertical and horizontal, for two configurations, partially filled with water and empty. The impulsive loads were created by impacting the torus with an instrumented 2.5-kg sledge hammer, and the hammer force and resulting torus motion were recorded using the T-DAC computer system.

A polyurethane cap was used on the hammer to cushion the impact sufficiently to excite only those modes with frequencies below 100 Hz. The impact force was measured with a quartz force transducer mounted between the cap and hammer head, and the transducer output was fed through a charge amplifier. Two velocity transducers were used to measure the response of the structure in the radial and vertical directions.

The modes of vibration were excited by impacting the structure at the 14 locations illustrated in Fig. 18. The transducer signals were recorded using a portable analog tape system, and then the tapes were played back and digitized using the T-DAC computer system. During the digitizing process the analog signals were amplified by a factor of 100, filtered at 250 Hz (eight-pole Bessel), and sampled at 1000 Hz. This choice of sampling parameters allowed accurate analysis of frequencies up to 100 Hz. Since the T-DAC computer system is transportable, it is usually not necessary to use the intermediate step of recording the data on analog tape. However, it was used in this case, since there was not a sufficient amount of sheltered space at the site to house the computer.

The modal analysis software was then used to combine the experimental data with the conceptual model to reveal the natural frequencies and mode shapes of seven modes of vibration below 100 Hz.

Figure 19 is a composite of three orthogonal views of a typical mode, at 25.9 Hz in this case. The dotted lines in the figure represent the "at rest" position of the torus, and the solid lines illustrate the

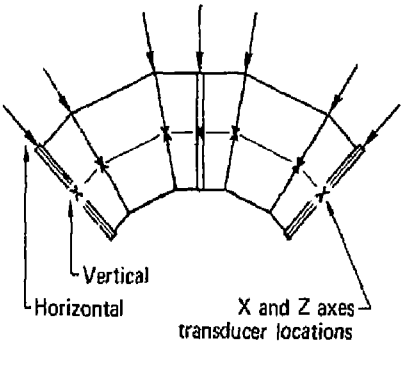

Fig. 18. Vertical and horizontal impact locations on the pressure suppression experiment torus.

mode shape. This mode appears to be the first bending mode of the torus.

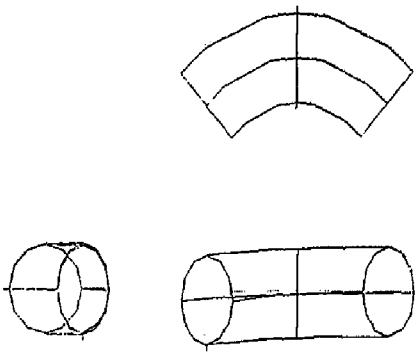

Fig. 19. The 25.9-Hz mode of the one-fifth-scale pressure suppression experiment torus.

Shiva Target Frame

The T-DAC system was transported to the laser facility target room to analyze the vibration modes of the Shiva target frame. At this time the frame construction had just been completed, and it was necessary to survey the structure to detect any possible significant vibration problems that might degrade the aiming system accuracy of the laser. The analysis was conducted in two phases. First, the background vibration of the frame due to seismic and building noise sources was measured using the data-acquisition function of the T-DAC system. Second, a modal analysis of the frame was conducted.

The modal analysis data were collected by placing a velocity transducer on a top corner of the frame as shown in Fig. 20. A person in a one-man bucket hanging from the ceiling hoist impacted the structure with a sledge hammer at 18 locations on the face of the frame.

The modes of vibration were determined from the impact data. The first two modes are illustrated in Fig. 21. The 3.8-Hz mode appears to be simple rocking of the frame, while the 11.9-Hz mode resembles a beam-bending mode. A spectral analysis of the background vibration levels was then combined with the modal analysis results to determine angular vibration levels at important locations on the target frame. In addition, simultaneous vibration noise measurements were made on the physically separate amplifier and target frames. These data were used to determine relative motion amplitudes between the two structures. All vibration measurements were found to be within the required operating tolerances.

Summary

Integration of sophisticated data-acquisition and data-reduction capabilities in the T-DAC computer system provides a powerful tool for the rapid modal analysis of complex mechanical structures. The T-DAC system can be easily transported to the vicinity of immovable structures. The transient-capture unit can be connected to a wide variety of vibration transducers for the measurement of impact response. The use of an easy-to-set up instrumented hammer to apply force inputs to a structure and the ability to immediately review the collected data on the T-DAC allows for rapid data acquisition. The use of a three-dimensional animated display provides quick and meaningful presentation of the analysis results. Thus, meaningful results can often be obtained in one day of field work.

Future efforts are directed at the application of more accurate techniques of modal parameter extraction and the investigation of possible links to existing dynamic simulation codes.

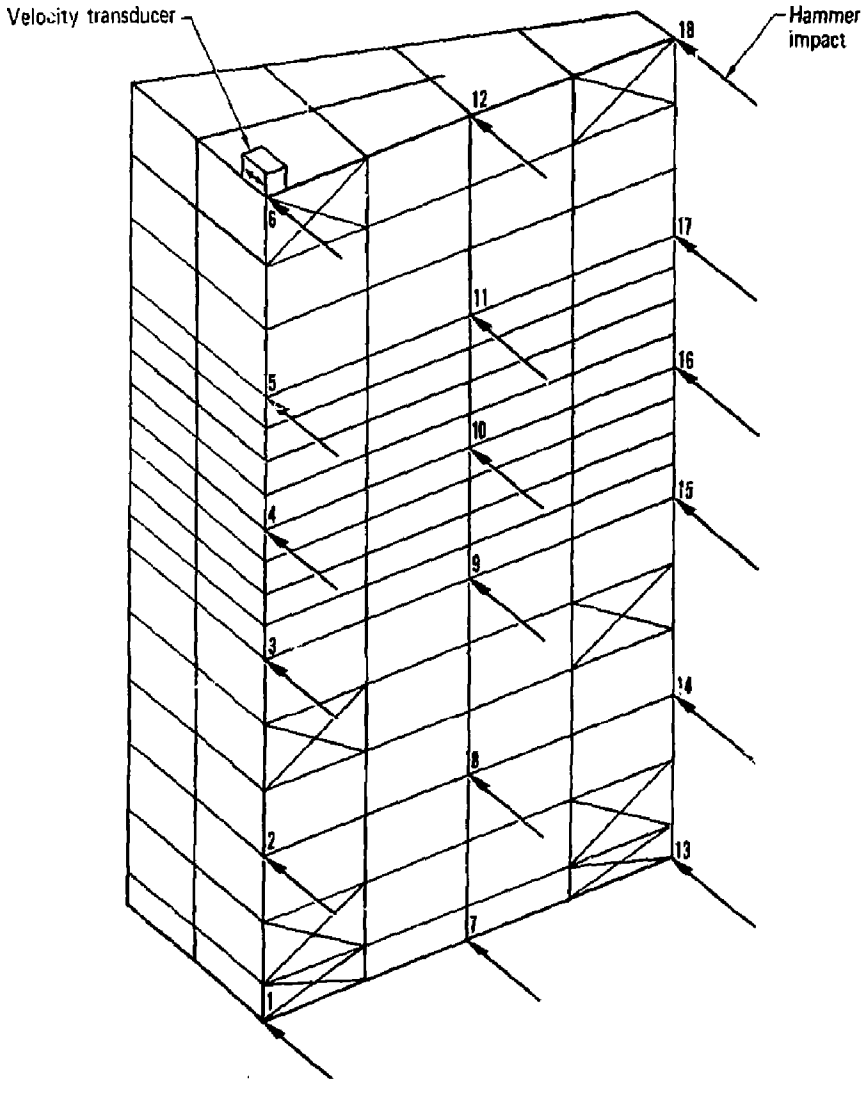

Fig. 20. A segment of the Shiva amplified frame showing the 18 hammer-impact locations and the placement of the velocity response transducer.

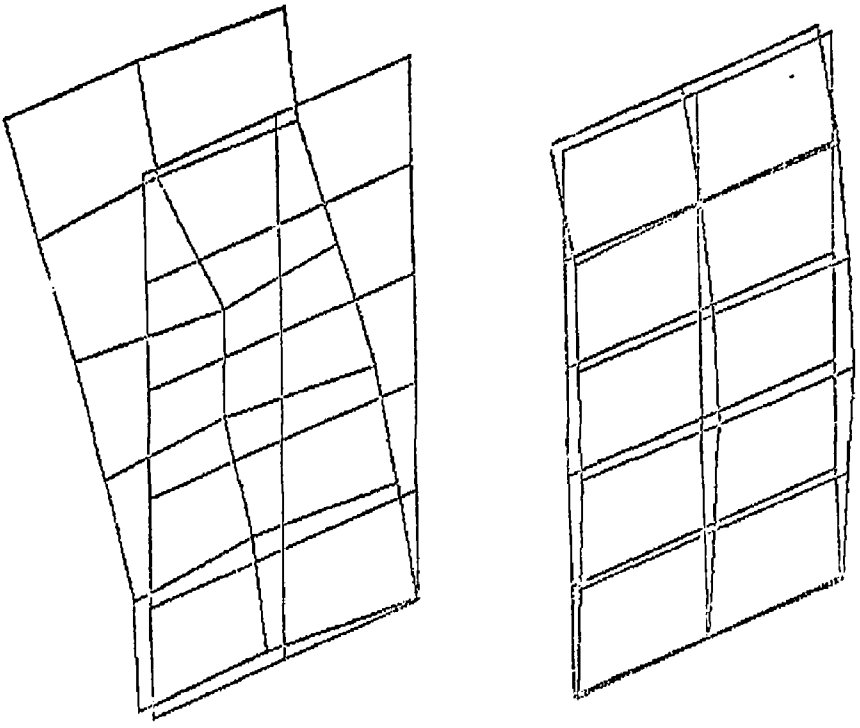

Fig. 21. Principal target-frame modes of vibration.

DETERMINATION OF SOUND VELOCITY ACROSS THE DIAMETER OF A LIQUID METAL COLUMN

We were asked to develop a method for measuring sound velocity in liquid metals for use with the LLL isobaric expansion apparatus.[23] In experiments using this apparatus, a 1-mm-diameter, 25-mm-long wire specimen is rapidly resistively heated u' 'er high-pressure argon gas. Measurements must ›rded quickly in the few microseconds following ›ecimen melt, before instability and breakdown of the molten column occur. The apparatus allows simultaneous determination of pressure, density, enthalpy, temperature, and electrical resistivity, which can be used to determine the specific heat and bulk thermal expansion coefficient of the liquid. Measurement of sound velocity was desired to allow additional determination of thermophysical properties for liquid metals, including the Grüneisen parameter, the specific heat at constant volume, and the adiabatic and isothermal compressibility of the liquid metal.

During the past two years, we have been developing a method of measuring sound velocity in liquid metals and felt it could successfully satisfy these needs. We found available techniques using piezoelectric transducers[24] unsuitable due to the need for thick, flat, and smooth specimens, and long measurement times as well as to the inability of the transducers to survive at extreme temperatures. So we successfully developed a noncontact technique that does not require transducers and can be used with very short experimental times and at very high

temperatures and pressures. This technique employs pulsed laser deposition loading and displacement interferometry. Briefly, a high power, Q-switched neodymium-glass (Nd-G) laser beam is focused on one side of the specimen, initiating a stress pulse traveling across the diameter.[25,26] The stress pulse arrival on the opposite side of the specimen diameter is recorded with a Michelson displacement interferometer using the specimen surface as the moving mirror. A closeup view of the mounted specimen and laser beams is shown in Fig. 22. The measured transit time of the stress pulse and the diameter of the metal column leads directly to the sound velocity.

Experimental Procedure and Considerations

Our first effort was to set up the optical system and calibrate it for accurate time interval measurements. As the transit time is only several hundred nanoseconds, inherent delays in the scope triggering and vertical input, transit time through the photomultiplier tube, electrical and optical path travel time, and effective start time of the stress pulse can have a significant effect on the measured transit time of the stress pulse through the diameter of the specimen. The timing was calibrated by using thin plate of high-purity oxygen-free copper of known dilatational velocity as the specimen. A 5% beam-splitter was placed in the high-energy laser beam to provide a fiducial marker, which was superposed on the photomultiplier signal output from the interferometer. This procedure eliminated all timing considerations except the difference in optical path lengths. Results were recorded using a high-frequency-response oscilloscope. The details of the timing calibration are shown in Fig. 23. The optical path from the first beam-splitter to the photomultiplier tube is 0.46 m shorter than the air path via the interferometer, so the Nd-G laser pulse appears 1.5 ns early on the oscilloscope record shown. We used an average value for the velocity of sound at room temperature for copper of 4740 m/s for compressional waves in an infinite medium.[27] The copper plate was 0.91 mm thick, so the expected transit time was 192 ns. The apparent time of start of the stress pulse on the record is obtained by measuring back 190.5 ns from the breakout of the interferometer signal, as indicated by the arrows. It is seen that the effective time of stress wave initiation is very near the beginning of the Nd-G laser pulse. The nominal sweep rate shown is 50 ns/cm. The results appear to be repeatable to within $\sim\pm 5$ ns.

We had to make a compromise in choosing the spot size used for the energy deposition on the 1-mm-diameter specimen rod. A very precisely focused spot results in a sharp signal arrival, but the peak displacement amplitude is greatly reduced because energy from the Nd-G laser is expended in drilling a hole in the specimen. A broadly focused beam on the other hand leads to a strong displacement signal, but signal arrival becomes distorted.

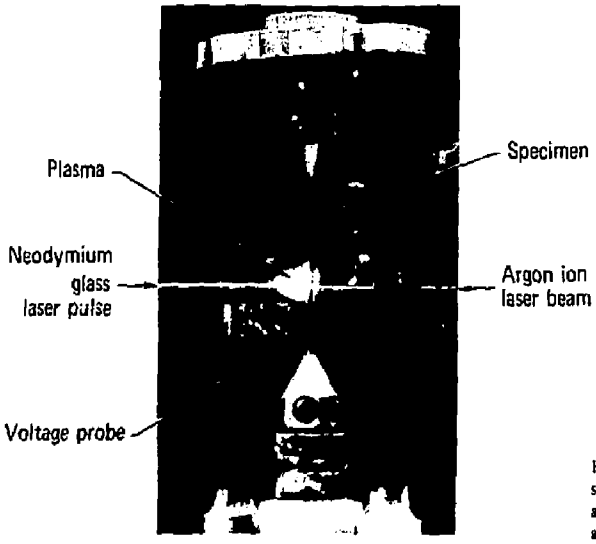

Fig. 22. Closeup view of 1-mm-diameter specimen showing high-energy laser beam and plasma blowoff on left side of specimen and interferometer laser beam on right side.

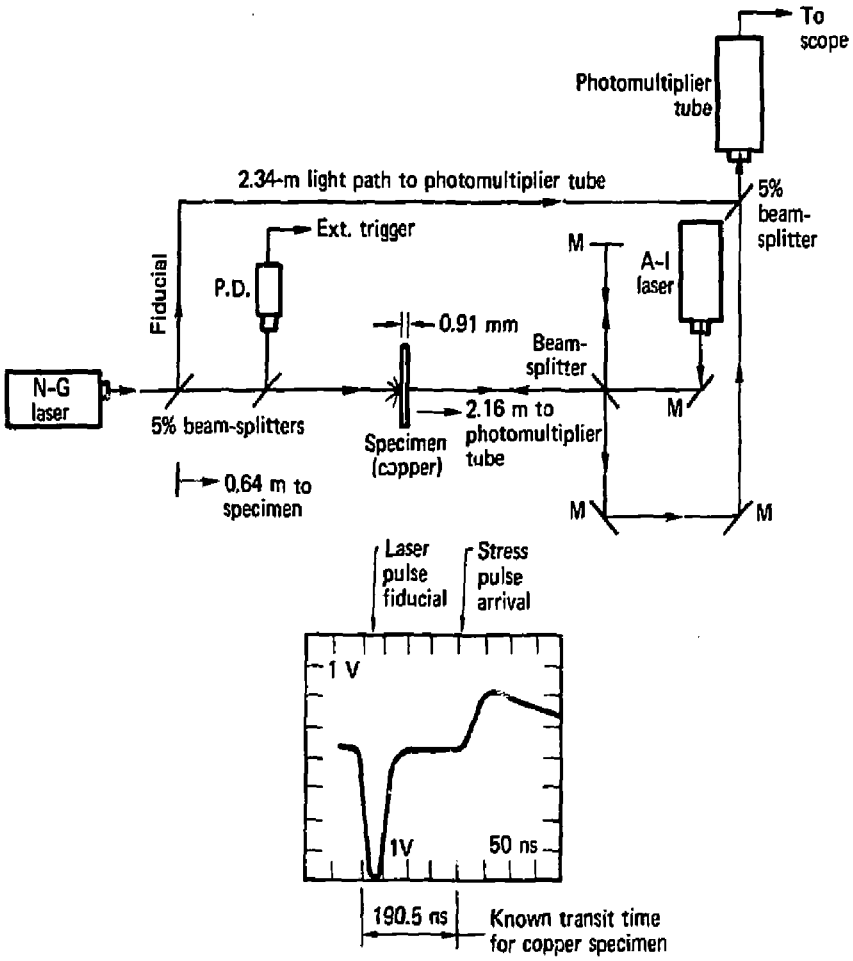

Fig. 23. Stress-initiation time calibration.

The best compromise for 1-mm-diameter samples appears to be a spot size of ~0.2 mm diameter.

The interferometer was adjusted so that the two arms had nearly equal path length and beam intensity. This results in large, high contrast fringes at the photomultiplier tube. The displacement signal sensitivity depends upon the position of the fringe pattern at the precise instant of the test. If it is close to a maximum or minimum, the sensitivity is low. This problem can be eliminated by using a quadrature system with the second signal shifted 90° so one detector will always respond at high sensitivity.

To test the technique in our lab, we fabricated an aluminum mock-up of the inner portion of the isobaric expansion pressure cell. This held the sapphire pressure windows and one of the sample-holding anvils complete with electrodes and cylindrical current return cap used in the actual system. A top view of the mock-up pressure cell containing the 1-mm-diameter specimen is shown in Fig. 24 with the associated optical setup. The energy from a high-power, Q-switched Nd-G laser (5-7 J, 30 ns) is directed through collimating aperture (1), a sapphire pressure window (2), and then is focused by lens (3) on a spot (0.2 mm diameter) on the surface of the 1-mm-diameter cylindrical sample (4). A stress pulse is generated in the sample by surface pressure produced from plasma blowoff.

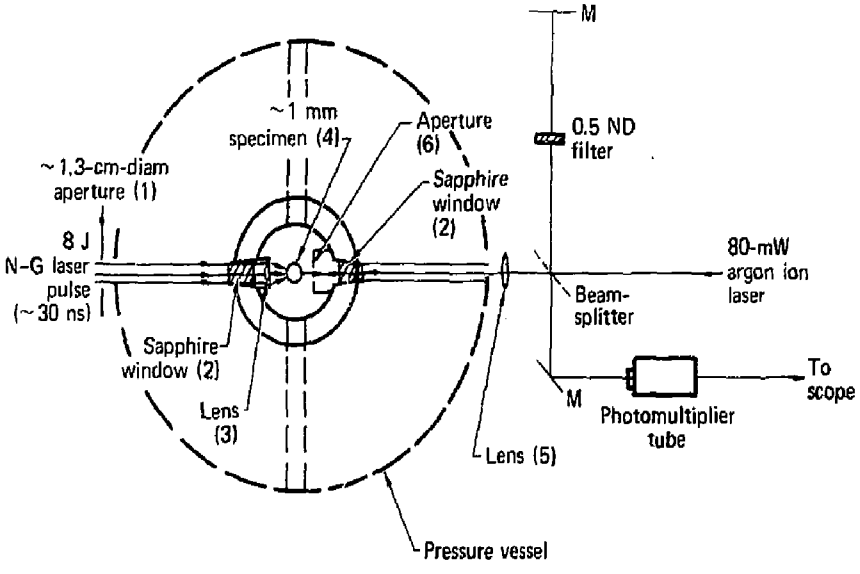

Fig. 24. Top view of isobaric expansion pressure cell and optical arrangement for sonic velocity measurements.

The stress pulse propagates to the diametrically opposite surface which acts as the moving mirror of the Michelson interferometer. Light from an argon ion laser is directed through lens (5), the sapphire window (2), aperture (6), and focused on the sample (4). The laser beam reflection is combined with a reference beam from the other leg of the interferometer. The sudden fringe shift produced in the interferometer when the stress pulse arrives is observed with a pulsed photomultiplier tube. The time of energy deposition is determined from a fiducial generated as described in the timing calibration (Fig. 23). The transit time for the pulse is determined by displaying the signals on a fast oscilloscope. The samples diameter during the transit time can be accurately determined from a streak camera record so that the propagation velocity can be calculated. The energy density deposited by the Nd-G laser must be restricted so that the weak shock wave generated will have a velocity close to the longitudinal sound speed.

A variety of solid metals were tested in the mock-up system including tungsten, tantalum, copper, iron, and lead. The principal operational differences were due to the different reflectivities and surface conditions of the samples. Adequate interferometric fringes for reasonably good signal-to-noise data were obtained for each solid metal. The accurate location of the high-energy deposition spot directly opposite the spot viewed by the interferometer was found to be very important. The stress pulse amplitude is rapidly reduced if this alignment is not good and the distance traveled by the stress pulse becomes different from the specimen diameter.

Liquid Lead Test

To check out the method for sonic velocity measurement in liquid metals, we selected lead specimens for testing due to the relatively low energy required to obtain melt. Experiments were first conducted on solid lead rods and subsequently on lead rods liquefied by the high current pulse from a 20-kV capacitor bank discharge. The stress transit time measurement was made a few microseconds following melt. Typical scope traces are shown in Fig. 25 for the solid and liquid lead tests. As in the calibration, the fiducial is simply a representation of the timing of the high-energy laser pulse. The measured sonic velocity for the solid specimen is reasonably close to an average value of 2.21 mm/μs taken from Ref. 27. As would be expected, there is a considerable drop in velocity for the liquid lead test. The measured liquid-lead sound velocity of 1.80 mm/μs agrees very well with a published value at melt of 1.78 mm/μs.[28]

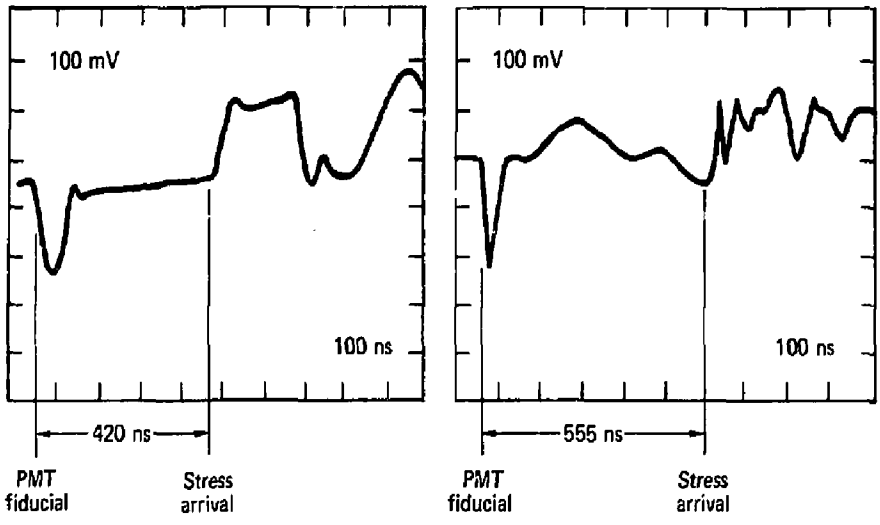

(a) Solid lead specimen (1.0 mm diam).
Measured sonic velocity = 2.38 mm/μs.

(b) Liquid lead specimen (1.0 mm diam).
Measured sonic velocity = 1.80 mm/μs.

Fig. 25. Oscilloscope trace data for sonic velocity measurements in solid and liquid lead specimens.

Conclusion

The noncontact method described using laser energy deposition and displacement interferometry provides a unique method for the measurement of sonic velocity in liquid metals yielding information not obtainable by conventional techniques. This capability is currently being installed in the LLL isobaric expansion experiment apparatus, where it will provide a more complete determination of the thermophysical properties of liquid metals.

TECHNICAL NOTES

The Effect of Strain-Gage Surface Preparation Techniques on Beryllium *(J. W. Hughes, Jr., Materials Engineering Division, and James Hanafee, Chemistry Department)*

Beryllium is a metal sensitive to machining damage, which can cause a loss in mechanical properties. Since some mechanical abrading is often used in surface preparation for mounting strain gages, it is desirable to know whether the abrading produces flaws. Metallographic study of beryllium subjected to four different surface-preparation methods was carried out.

The beryllium was impact attritioned and isostatically pressed (pressing T209) commercially. It had an ultimate strength of 557 MPa, yield strength of 395 MPa, elongation of 3.9%, BeO of 1.8%, and grain size of 5 μm. Flat areas, approximately 25 mm square, were carefully ground on test coupons 1.27 mm thick. All effects of grinding damage were removed by chemically etching 0.076 mm off the surface.

The test coupons were then subjected to four surface-preparation procedures suitable for mounting a variety of strain gages. All coupons were washed with ethyl alcohol. For method 1 and 2, the coupons were then wet-abraded for 20 s with −320 grit sandpaper at light pressure. In method 1, the abrading was in a crosshatch pattern and in

method 2, in a random, circular pattern. Finally, both samples were rinsed with distilled water. In method 3, the sample was grit blasted with 25-μm silicon carbide for 20 s at a distance of 50 mm and then rinsed with distilled water. In method 4, the sample was grit blasted with 50-μm silicon carbide for 20 s at a distance of 50 mm and then rinsed with distilled water. All abrading and grit-blasting preparations were conducted under wet or enclosed (non-hazardous) conditions.

Following the strain-gage surface preparation, the specimens were cross sectioned and prepared for metallographic examination. Great care was exercised to avoid introduction of flaws at the edge of the specimen directly below the strain-gage preparation surface. It was particularly important to avoid the creation of twins.

Compared to a typical machining or grinding operation, the strain-gage surface preparation techniques are quite gentle. Thus, it may be expected that microcracks and gross plastic distortion would not be present, and, indeed, such evidence of major surface damage was not found. The primary concern was the creation of twins (intergranular mechanical deformations). None of the four surface-preparation methods caused a significant amount of twinning.

In conclusion, the gentle abrading necessary for affixing strain gages produced a negligible density and depth of flaws and did not lower the mechanical properties of beryllium.

Design of D-38 Burn Box *(F. Holdener and I. Murray, Materials Engineering Division, and R. Samuelson, Weapons Engineering Division)*

We have designed a burn box for disposal of depleted uranium. As a common constituent of many weapons, this material is machined into many shapes at LLL. It is a low-alpha-emitting metal that provides few handling problems as stock material or finished parts. However, the transition from stock to part reveals a nasty characteristic requiring special handling techniques. Given the correct shape and size, depleted uranium, like magnesium, becomes pyrophoric. Chips, spirals, and coils generated by machining will, with little provocation, burst into flame releasing toxic fumes as well as heat. Several precautions were developed to avoid this problem during machining. However, no method was available for the disposal of the accumulated scrap. This problem had been examined for some time. When we started our design work in October 1976, the LLL inventory of depleted uranium scrap stood at 100 barrels, each containing approximately 50 kg of metal. On the average, three barrels are generated each month so that a satisfactory disposal method was crucial.

Depleted uranium in this form has insufficient value to warrant reprocessing. Shipping the barrels to established burial or disposal sites was ruled out as coming too close to violating existing Department of Transportation rules for transporting hazardous materials. The material is pyrophoric when removed from water and when in water it generates a small amount of potentially explosive hydrogen gas.

Since the oxide of depleted uranium is relatively safe and requires minimal handling precautions, we solved the disposal problem by designing a box to oxidize or "burn" the scrap under safe, controlled conditions. This box, shown photographically in Fig. 26, and schematically in Fig. 27, consists of three chambers. The first accepts the barrel in a yoke that rotates and dumps the contents into a drawer. A hose is available for washing the barrel clean. The bottom of the drawer is a stainless steel mesh that retains the bulk of the scrap. The liquid and very small pieces of scrap pass through onto a replaceable, consumable filter after which the liquid is pumped into 0.21-m^3 waste drums. The loaded drawer moves to the second chamber where it is ignited. Air or argon is fed to the chamber through control valves to allow precise control of burning rate. A water-cooled heat exchanger above the burn drawer transfers the heat of combustion to the building's low conductivity water system. A second drawer with a solid bottom receives the ash as it falls through the burn drawer bottom. This transfer is aided by a vibrator attached to the second chamber. The oxide drawer then moves into the third chamber where the uranium oxide may now be safely bagged for subsequent shipment to a Nevada burial site. A complex control and filtering system maintains negative pressure in the box at all times and prevents uncontrolled burning rates. All air and combustion gases pass through high-efficiency filters before entering the building's exhaust system.

This box is now being developmentally tested and should be completed this spring. Once in operation, it should be able to process all existing stockpiled scrap within 6 months and then require only monthly use thereafter.

Developmental Work on Multifrequency Holographic Contouring *(D. Boyd and B. Maxfield, Materials Engineering Division)*

The Weapons Program frequently encounters problems where surface profiles must be determined very accurately (within a few micrometers).

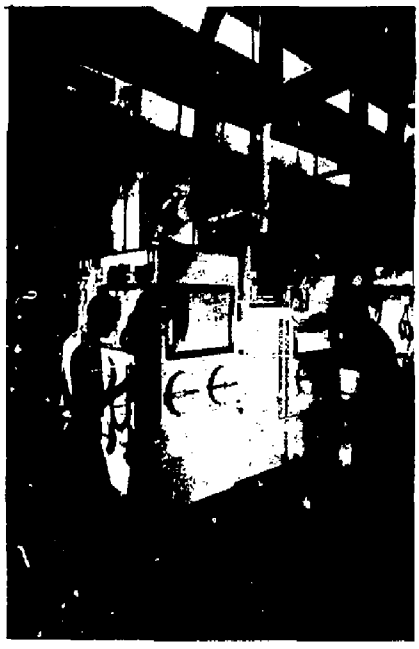

Fig. 26. D-38 burn box.

Although mechanical contact methods are presently the only technique having sufficient accuracy, an optical means of measuring the surface profile (contouring) is desirable. Such methods have two important advantages. First, only visual rather than mechanical contact with the object is required. This permits the contouring of hot, radioactive, or toxic objects where mechanical contact is either impossible or undesirable. Second, the entire body is contoured rapidly and simultaneously. Recording times ranging from a few seconds to possibly microseconds are possible. This makes measurements relatively free from changes caused by the environment and may even permit dynamic contouring.

Holographic interferometry is the only optical method which can in principle achieve the required resolution for surface contouring of weapons. It is extensively used for measuring small changes in surface position, but has been used very little as a tool for surface contouring due to unsolved problems relating to its use. We are working to solve these problems because of the potential applications of holographic interferometry in weapons machining. In particular, we are interested in multifrequency holographic contouring (MFHC) because it can be used when total liquid immersion must be avoided, as is often the case for weapons materials and assemblies.

Our work thus far has involved using reported methods of MFHC under the conditions that exist in engineering-type environments and pinpointing problems with such applications. A description of the technique is needed to understand the problems. Briefly, MFHC and other optical surface contouring methods superimpose a set of optical interference fringes on the surface of an object. The fringe or contour interval is determined by both the optical geometry and wavelength. Fringes result from interference between two slightly different images of the same object. Changing either the refractive index of the medium surrounding the object or the measuring wavelength (frequency) between exposures will produce the required images.

Several disadvantages of using MFHC as a contouring tool for real surfaces have been identified as requiring further study before MFHC will find widespread use as a contouring tool. First, fringe contrast is low. Contrast is often improved by using surface coatings to give highly diffuse reflectivity, but for many of our applications the surface cannot be altered in any way. By improving exposure techniques, we have made high-contrast holograms of D-38 objects with aged and fresh surfaces. Second, more convenient methods for working with high fringe density must be developed since high-resolution surface contouring nearly always results in fringe densities that cannot be resolved by the unaided eye. Third, different optical geometries must be developed in order to handle complexities associated with the wavelength dependence of many optical components of the interferometer.

We believe the contour maps generated by MFHC have other important applications beyond machining. These include the monitoring of long-term surface effects and the measurement of strain. Comparison of contour maps made at various time intervals during a wear process or fatigue cycle of an object could be used to monitor changes in surface shape.

Using contour maps as a strain measurement technique involves the superposition of two sets of contour fringes. Differences between these contour maps yield the strain. Because the contouring interval can be varied, MFHC would provide a wide field of view strain gage with variable sensitivity. We are continuing our development of noncontact MFHC contouring methods for use on as-machined surfaces. Future plans include investigating other applications of holographic contouring.

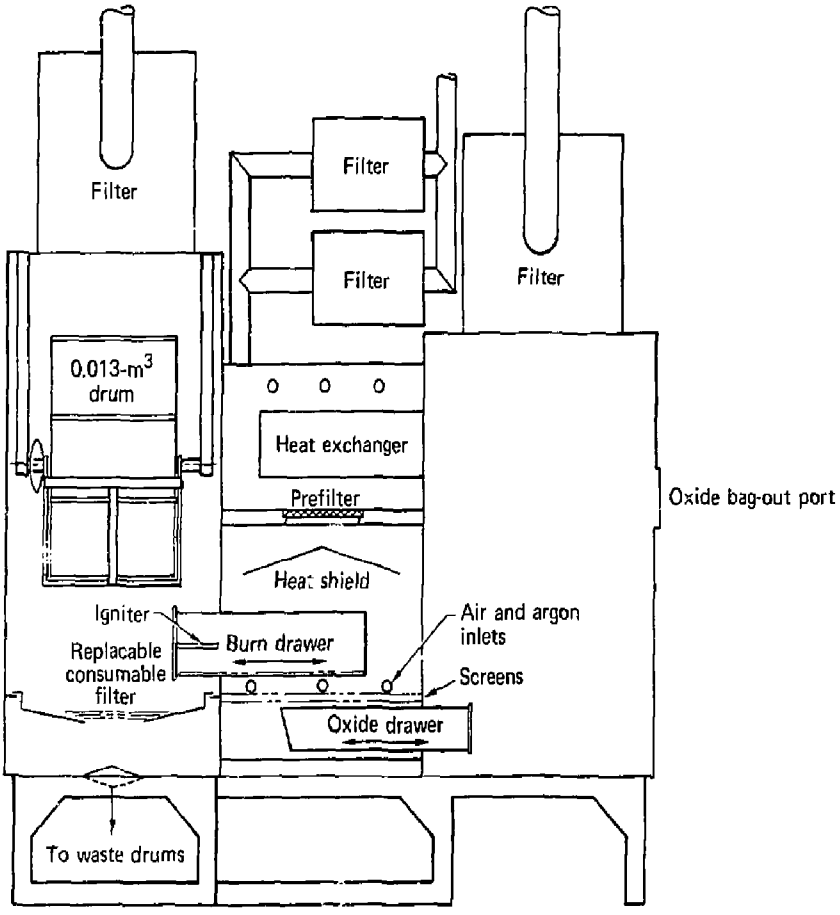

Fig. 27. Schematic of major burn box components.

Fracture Mechanics Studies Performed in the Materials Engineering Division *(Manuel Prado, Materials Engineering Division)*

The Materials Engineering Division (MED) performs fracture mechanics studies to assess the ability of materials to resist brittle, unstable fractures. The relatively new engineering discipline of fracture mechanics arose when designers using high-strength materials found that failures occurred at levels substantially below the design stresses. These failures were usually rapid, unstable fractures of the type normally referred to as brittle fractures.

In MED, we perform fracture mechanics studies for those programs where unstable crack growth can appreciably affect the performance of the system. For example, we have tested the toughness of components used at the Nevada Test Site, done materials evaluations for the Weapons Program, and assessed the crack resistance of superconducting magnets used in the Magnetic Fusion Energy Program. We also routinely test materials used in new pressure vessels to be sure that their toughness minimizes the probability of brittle fractures.

We perform two classes of fracture mechanics studies: (1) impact tests, which give a relative measure of material toughness, and (2) pull or flexure tests, which measure plane strain fracture toughness. A common impact test uses the

traditional Charpy V-notched specimen to obtain temperature transition curves that give the engineer or designer a relative measure of material toughness. Other impact tests include the dynamic tear test (Fig. 28), which is similar to the Charpy impact test, and the drop weight test, which gives the temperature at which a material begins to exhibit ductile behavior.

Pull or flexure tests measuring the plane strain fracture toughness of the material must be performed if an analytical approach to fracture prevention is desired. With this material parameter, the engineer can calculate the maximum crack size that can exist within the structure without causing catastrophic structural failure.

Presently we are investigating other methods of assisting the analyst in predicting fracture behavior. We are working on elastic-plastic concepts, crack arrest, and dynamic material characteristics. These tests assist the analyst and designer in determining acceptable flaw sizes or in selecting a material in which the probability for unstable crack propagation is remote.

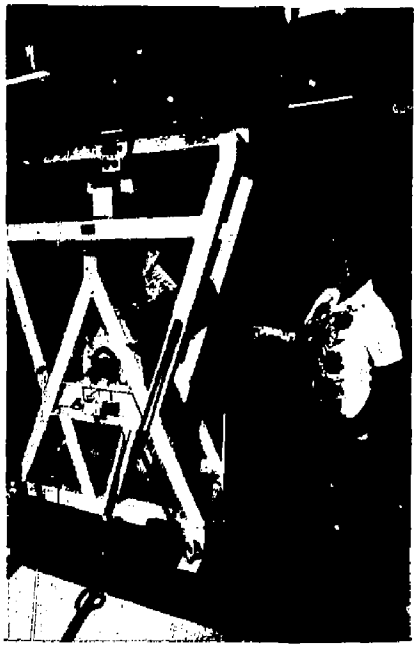

Fig. 28. Double-pendulum dynamic tear machine. Operator is placing specimen in anvil. When she releases the trigger, both pendulums will rotate in the direction shown to break the specimen. The energy absorbed in breaking the specimen is recorded on the dial and gives an indication of material toughness.

Instrumenting a Pressure Suppression Experiment for a Mark I Boiling Water Reactor—Another Measurements Engineering Challenge *(W. M. Shay and T. B. Miller, Materials Engineering Division, and W. G. Brough, Electronics Engineering Division)*

We successfully instrumented a Mark I boiling water reactor pressure suppression system, built to one-fifth-scale at Livermore in 1977.[29] The extremely high, laboratory-type accuracies required under field conditions made our work a measurements engineering challenge. Seven types of transducers were used to obtain high-accuracy, dynamic loading data during a hypothetical loss-of-coolant accident.

The prime measurement for this experiment was the vertical loads in the suppression system during a simulated loss-of-coolant accident. These were measured in two ways: by load cells supporting the one-fifth-scale suppression system and by integrating the pressure-time history of pressure transducers installed on the suppression system.

Our effort included selecting and calibrating each transducer, putting together a data acquisition system, installing all the transducers on the various components, and supervising the monstrous data reduction effort (approximately 1400 engineering data plots were generated for the 27 air tests already completed) all within a short time scale.

All transducers were designed and selected for the thermal transients that would be encountered in the steam phase of the experiment. Each transducer was thoroughly static-calibrated to insure that those fielded actually met the rigid performance requirements of this experiment. A multiplexing data acquisition system capable of recording 200 plus data channels was used. Special steps were taken to insure as noise-free data as possible.

Throughout our work, accuracy was our major concern. The total end-to-end error (from the transducer to the final data plot) had to be less than or equal to ±2% of the fullscale range set on the data acquisition system. To determine the accuracy of the data, we subjected approximately 50% of the transducers to accurately known inputs. We found that 88% of the transducers checked achieved total errors of 2% or less. This total error was achieved with transducers from 5 different manufacturers whose "quoted" static error bands differed by a factor of approximately 16.

Thus far, 27 air tests have been completed with an average of 175 transducers recorded for each test. The instrumentation worked well and results have been excellent. Steam tests are scheduled during fiscal year 1978.

PUBLICATION ABSTRACTS

K. L. Steffan, *High-Velocity Impact Tests Involving Thin Spherical Shells of Tantalum and 304 Stainless Steel,* Lawrence Livermore Laboratory, Rept. UCID-17546 (1977).

This experimental program generated data to improve computer-code modeling of impact phenomena. The improved computation technique will be used to design a fissile-material container able to withstand a 335 m/s impact. The program involved flyer-plate-impact tests using thin shells of annealed 304 stainless steel and annealed tantalum at impact velocities of 28-180 m/s. No active instrumentation was used in this study; instead, all data were derived from measurements of test specimens. Pre- and post-test measurement of interior and exterior dot patterns etched on the shells provided surface-strain information. Radiographs of the deformed shells provided shell-contour data that we plotted vs impact velocity. Curves were fit to these data. We found that normalized crush height varies almost linearly with impact velocity for both materials, that normalized radius of contact varies directly with impact velocity for both materials but appears independent of shell thickness for tantalum, and that normalized interior-fold radius varies inversely with impact velocity and directly with shell thickness for stainless steel, but no clear relationship appears for tantalum.

S. R. Vosen, D. J. Bender, J. H. Fink, and J. D. Lee, *Mechanical Design Criteria for Continuously Operating Neutral Beams,* Lawrence Livermore Laboratory, Rept. UCID-17573 (1977).

M. R. Posehn, *TCD: A Program for Acquisition of Thermocouple and Other Slow-Speed Data,* Lawrence Livermore Laboratory, Rept. UCID-17586 (1977).

A special applications code called TCD is used on the T-DAC computer system at LLL in order to acquire slow-speed data from tests and experiments. This report describes the capabilities and details of operation of TCD.

D. F. Arthur, *Dynamic Response Analysis of the PSE Torus,* Lawrence Livermore Laboratory, Rept. UCID-17594 (1977).

This paper describes a structural dynamic analysis of the 1/5-scale toroidal wetwell. The subscale toroidal wetwell is part of the Pressure Suppression Experiment Facility at Lawrence Livermore Laboratory. The analysis objective is to show that experimental structural loads measured by load cells in the wetwell supports are consistent with the internal hydrodynamic forcing function measured by pressure transducers. Finite element analysis of the wetwell indicates that the load and pressure measurements are consistent.

J. H. Pitts, *Mass Flowrates Through the Vent Lines During Air Tests of the 1/5-Scale Mark I BWR Pressure Suppression System,* Lawrence Livermore Laboratory, Rept. UCID-17601 (1977).

Mass flowrates per downcomer show that the three vent lines connecting the drywell to the toroidal wetwell test sections are matched within 10% on 19 of 23 applicable air tests. Vent line flow coefficients determined for the first 0.3 seconds after the start of drywell pressurization are within 20% of calculated values.

J. W. Sterbentz, *Mark I 1/5-Scale Boiling Water Reactor Pressure Suppression Experiment Comparison of Experimental Data to an Analytical Computer Model,* Lawrence Livermore Laboratory, Rept. UCID-17605 (1977).

This report was designed to compare graphically the experimental data from the Lawrence Livermore Laboratory's 1/5-scale Boiling Water Reactor Pressure Suppression Facility with the computer model, CONTEMPT-LT. The comparison involves the transient pressure behavior in the drywell and the 7.5 and 90 wetwell sectors. All tests used in the comparison were conducted with a perfect gas (no steam tests). Specifically, the experimental air clearing tests were driven by pressurized nitrogen (N2) gas. The comparison was done for tests involving variable drywell overpressure, drywell pressurization rate, downcomer submergence and different geometries using restricting and blind orifices in the vent pipes. The results indicate that the major parameters effecting the correspondence between the experimental data and CONTEMPT-LT are the drywell pressurization rate and the restricting orifice plates.

J. W. Sterbentz, *Calculated Volumes and Internal Surface Areas Mark I 1/5-Scale BWR Pressure Suppression Facility (LLL),* Lawrence Livermore Laboratory, Rept. UCID-17606 (1977).

This report contains calculated volumes and internal surface areas for the vent pipes and ringheader assemblies from the Mark I 1/5-Scale Boiling Water Reactor Pressure Suppression

Facility. Specifically, the calculated volumes and surface areas included the component sections of the vent pipes, ringheader and downcomers in both the 7.5° and 45° torus sectors. The total volumes (vent pipe, ringheader and downcomers) for the 7.5° sector and 45° sector are 0.076 m^3 (2.68 ft^3) and 0.575 m^3 (20.3 ft^3), respectively. The total internal surface areas (vent pipe, ringheader and downcomers) for the 7.5° sector and 45° sector are 1.85 m^2 (19.9 ft^2) and 7.30 m^2 (78.7 ft^2), respectively.

D. J. Bender, J. D. Lee, and R. W. Moir, *Preliminary Assessment of a Symbiotic Fusion-Fission Power System Using the TH/U Refresh Fuel Cycle*, Lawrence Livermore Laboratory, Rept. UCID-17607 (1977).

R. W. Young, J. O. Hallquist, and G. L. Goudreau, *HONDO Code Upgrade*, Lawrence Livermore Laboratory, Rept. UCID-17611 (1977).

Under the provisions of contract W-7405-Eng-48, Lawrence Livermore Laboratory has added a contact-impact algorithm to a finite element code used by the United States Army Engineer Waterways Experiment Station. As now structured, the code can solve problems with material interfaces that slide but do not penetrate; tied material interfaces that do not slide but allow unequal zoning across the interface; material interfaces with voids that open or close, and with sliding contact either with or without friction; and intersecting material interfaces with any combination of the properties stated above.

This report provides the information needed by users of the contact-impact algorithm.

Results from three numerical examples are included to illustrate the effect of varying the level of interface restraint.

D. J. Bender, J. D. Lee, and R. W. Moir, *A Perspective on the Fusion-Fission Hybrid Reactor*, Lawrence Livermore Laboratory, Rept. UCID-17622 (1977).

J. H. Pitts, *1/64 Scale Model Tests of a Mark I Boiling Water Reactor Pressure Suppression System*, Lawrence Livermore Laboratory, Rept. UCID-17625 (1977).

Results of air blowdown experiments, conducted on a detailed 1/64 scale model of a Mark I BWR pressure suppression system, show no difference in observed phenomena between tests with the full 360° toroidal wetwell and tests with a 90°, 45° or 22-1/2° sector of the toroidal wetwell. Phenomena observed qualitatively on the 1/64 scale apparatus had the same characteristics as those observed in later tests on the 1/5 scale apparatus.

Bubble action and pool swell were largest in regions where the downcomers were closely spaced. Blocking one of the eight vent lines had insignificant effects on the results.

D. W. Coats, *Stiffness and Flexibility Element for SAP4*, Lawrence Livermore Laboratory, Rept. UCID-17654 (1977).

A stiffness and flexibility element has been added to the SAP4 program at the Lawrence Livermore Laboratory. Direct input of a member stiffness or member flexibility matrix is now possible. This element can be used to significantly reduce the number of degrees of freedom in a large mathematical model by representing a portion or portions of the structure with one or more of these elements.

W. Lai and E. W. McCauley, *BWR Mark I Pressure Suppression Study—Bench Mark Experiments*, Lawrence Livermore Laboratory, Rept. UCID-17661 (1977).

W. Lai and E. W. McCauley, *BWR Mark I Pressure Suppression Study—Effect of Downcomer Fill Level on the Vertical Load Function*, Lawrence Livermore Laboratory, Rept. UCID-17662 (1977).

D. L. Bernreuter and L. H. Wight, *Analysis of Diablo Canyon Site Response Spectra*, Lawrence Livermore Laboratory, Rept. UCRL-52263 (1977).

The Diablo Canyon Nuclear Power Plant, located on the central California coast, is nearing completion. Recent geologic and seismological investigations have indicated that the nearby Hosgri fault may be part of a major fault system. If so, the original Design Basis Earthquake (DBE) may be inadequate for Diablo Canyon. Therefore, we have examined several factors that could significantly affect the design response spectra for the site. We find that, because of the area's geology, significant site effects could occur that would reduce ground motion; possible soil-structure interaction would also reduce the seismic motion at the basemat of the main structure as compared to the free-field motion. Studies of wave-passage effects have shown that they are complicated and cannot be easily predicted. "We conclude that an increased-magnitude DBE should have little effect on the reactor design if the increase is caused by greater fault rupture length rather than increased stress drop."

S. B. Sutton, *An Investigation of Pressure Transient Propagation in Pressurized Water Reactor Feedwater Lines,* Lawrence Livermore Laboratory, Rept. UCRL-52265 (1977).

This document reports the results of a study for the Nuclear Regulatory Commission (NRC) to provide a general understanding of pressure transient (water hammer) propagation in pressurized water reactor (PWR) steam generator feedwater piping systems. A typical feedwater network is defined, and pressure transient initiation is discussed, as well as the plausible pulse shapes reported. The analysis is performed by using the computer codes PTA and WHAM. Forces are calculated at elbows and valves by using momentum principles. The effects of pipe yielding, pipe wall friction, and elbow and value losses are included. Pipe yielding and elbow/valve effects are found to be important, and pressure magnitudes and forces are substantially reduced when these effects are included in the analysis. Typical pressure and force time histories are also given.

J. O. Hallquist and G. L. Goudreau, *SAPP—A Post-Processor for Two-Dimensional Finite Element Codes,* Lawrence Livermore Laboratory, Rept. UCRL-52318 (1977).

This report is a user's manual for the post-processor SAPP. SAPP reads the familied binary plot files generated by the two-dimensional finite element codes presently used at LLL, plotting contours, time histories, and deformed shapes. Contours of nearly 100 different quantities may be plotted on meshes consisting of triangular and variable node (4 to 8 nodes/zone) quadrilateral elements. SAPP can compute a variety of strain measures at either Gauss integration or nodal points. If desired, momentums can also be computed for each material.

D. A. Schauer, *Thermal and Dynamic Effects in Electron Beam Welding Cavities,* Lawrence Livermore Laboratory, Rept. UCRL-52331 Thesis (1977).

An experimental and analytical study of the temperature distributions along the molten metal surface in an electron beam welding cavity is described. Surface temperature distributions in cavities were measured with a narrow band infrared radiation pyrometer. The availability of the cavity temperature measurements allowed estimates to be made for the vapor pressure and surface energy forces as a function of cavity position. The results indicated a force imbalance occurred in the cavity. It is postulated that at the location of the force imbalance a liquid material projection forms periodically and moves into the path of the electron beam. The liquid in this projection is driven towards the bottom, partially filling the cavity. This action is followed by the electron beam pushing the liquid aside to form a maximum depth cavity. This process is then repeated.

An analysis for predicting cavity oscillation frequency shows reasonable agreement with frequencies measured at the weld root determined from weld sections. A study of the measured temperature distributions in cavities of varying depth combined with the force imbalance observations led to an interpretation of when spiking might occur. A procedure is proposed for determining the spiking tendency for a given set of weld parameters. The results of this study permit a designer to select *a priori* the best set of weld parameters to achieve a weld of predictable quality.

J. B. Holt, D. W. Hosmer, and R. A. Van Konynenburg, *Helium Generation in Copper by 14.8-MeV Neutrons,* Lawrence Livermore Laboratory, Rept. UCRL-76765 (1977). Submitted to the International Conference on Radiation Effects and Tritium Technology for Fusion Reactors, Gatlinburg, Tennessee, October 1-3, 1975.

High purity copper foils were irradiated with 14.8-MeV neutrons from the rotating target neutron source facility at LLL. The average energy of the neutrons was 14.75 ± 0.1 MeV, and the average fluence was 7.0×10^{16} n/cm^2. After irradiation each foil was heated to the melting point and the released helium was measured by a mass spectrometer of special design. Isochronal heating was carried out on several samples to establish the type and temperature of maximum release. Calculated cross sections from the literature for the (n,α) and $(n,n'\alpha)$ nuclear reactions were used, and the predicted amount of helium was consistently about 0.5 of that actually measured. Because there is very little data on helium generation in metals irradiated with high energy neutrons, these results are important and will be related to potential CRT materials.

P. B. Mohr, *Preliminary Design of a Subscale Ceramic Helical-Rotor Expander,* Lawrence Livermore Laboratory, Rept. UCRL-79523 (1977). Submitted to the Proceedings of the Fifth Army Materials Technology Conference, Newport, Rhode Island, March 21-25, 1977.

A program has been undertaken to develop a class of fuel-tolerant ceramic expansion engines believed to have the potential for operating reliably and efficiently on the unmodified combustion products of coal. Such engines, operating essentially uncooled at temperatures in excess of 1350°C, appear attractive for original and retrofit applications in automotive, propulsion, industrial, and especially topping-cycle service for central power stations. The demonstration of a first small-scale (125-mm rotor diameter) ceramic helical-rotor expander has been identified as an early and feasible program goal. This paper describes design concepts and preliminary designs being considered for the prototype. In addition to expander design, the initial program includes consideration of the key questions of expander performance, combustion-product tolerance, materials and component evaluation and development, along with planning for development to intermediate (600-mm) and power-station-scale (1600-mm) applications. Progress in these and other programmatic aspects is summarized briefly.

J. J. Lim and J. E. Wells, *Project Scheduling and Resource Leveling: An Algorithmic-Interactive Procedure,* Lawrence Livermore Laboratory, Rept. UCRL-79539 (1977). Presented at the Lawrence Symposium on Systems and Decision Sciences, Lawrence Hall of Science, Berkeley, California, October 3-4, 1977.

This paper presents a mathematical model of the resource-constrained scheduling problem. An algorithmic-interactive procedure for solving the problem is developed because the combinatorics of the mathematical model prevent an analytical solution. The procedure is shown to be a viable technique when applied to a scheduling and resource allocation problem at Lawrence Livermore Laboratory.

J. J. Lim and J. E. Wells, *An Algorithmic-Interactive Approach for Scheduling and Resource Smoothing,* Lawrence Livermore Laboratory, Rept. UCRL-79595 (1977). Submitted to the 1977 Symposium sponsored by the San Diego Section of ORSA, San Diego, California, September 23, 1977.

Conflicts often arise in allocating the resources in a multiproject, multiresource system. Consequently deciding which projects to delay or schedule becomes a problem. Furthermore, it is often desirable to keep the usage of the resources as smooth as possible. This paper presents a mathematical model of the resource-allocation problem. An algorithmic-interactive procedure for solving the problem is developed because the combinatorics of the mathematical model prevent an analytical solution. The procedure is shown to be a viable solution technique when solution results are compared with actual results after the procedure is applied to a scheduling and resource-allocation problem at Lawrence Livermore Laboratory. In this case, the procedure could have anticipated and alleviated many actual problem areas.

I. F. Stowers, *Advances in Cleaning Metal and Glass Surfaces to Micron Level Cleanliness,* Lawrence Livermore Laboratory, Rept. UCRL-79702 (1977). Presented at the American Vacuum Society Conference, Boston, Massachusetts, November 8-11, 1977.

A high pressure 6.9 MPa solvent spraying technique has been developed to remove small (>5 μm) contaminant particles from large (100 m^2) surface areas. Chemically polished and etched 304 stainless steel components are solvent sprayed to achieve cleanliness levels of less than 10 particle/cm^2 > 5 μm diameter. The high pressure and high liquid velocity cleaning technique is able to remove 99.9% of >5 μm diameter particles in 5-10 seconds. This compares with ultrasonic cleaning which removes only 20-60% of >5 μm particles in 2-10 minutes. High levels of particulate cleanliness are required for large solid-state laser systems where contaminants can migrate to optical surfaces and cause severe pitting. The pitted glass must be removed and repolished to maintain acceptable beam quality.

Special Class 100 clean room procedures and equipment have been developed to verify the cleanliness of the cleaned components and to ensure their remaining clean during installation and operation. Development of these cleaning procedures has resulted in greatly increased time between failures of solid-state disk laser amplifiers.

Although developed specifically for cleaning optical components, the basic technique should find wide application in any field requiring precision cleaned surfaces.

L. R. Pedrotti, *The Tokamak Fusion Test Reactor Neutral Beam Injection System Vacuum Chamber.* Lawrence Livermore Laboratory, Rept. UCRL-79706 (1977). Submitted to the Proceedings of the Seventh Symposium on Engineering Problems of Fusion Research, Knoxville, Tennessee, October 25-28, 1977.

Most of the components of the Neutral Beam Lines of the Tokamak Fusion Test Reactor (TFTR) will be enclosed in a 50 cubic metre box-shaped vacuum chamber. The chamber will have a number of unorthodox features to accommodate both neutral beam and TFTR requirements. This paper presents the design constraints, and the resulting chamber design.

L. C. Pittenger, *A Neutral Beam System for the Tokamak Fusion Test Reactor,* Lawrence Livermore Laboratory, Rept. UCRL-79707 (1977). Submitted to the Proceedings of the Seventh Symposium on Engineering Problems of Fusion Research, Knoxville, Tennessee, October 24-28, 1977.

The Tokamak Fusion Test Reactor will be installed at the Princeton Plasma Physics Laboratory facility. This is a major step to reach the goal of fusion power using toroidal magnetic fields for plasma confinement. A major part of this test reactor will be four neutral beam injection systems. These systems will inject 20 MW of 120 kV neutral deuterium atoms into the plasma for 0.5 seconds.

In order to achieve the required power input to the plasma, several systems are required within the neutral beam line. These are the source, neutralizer, ion deflection magnet, calorimeter and retraction system, ion dump, cryopumps and vacuum enclosure. All of these systems have constraints imposed which increase the complexity of their designs. Since all systems must operate in a tritium environment, remote handling capabilities must be incorporated into the design.

The paper presents an overview of the Lawrence Livermore Laboratory/Lawrence Berkeley Laboratory Neutral Beam Injection System design. Specifications for the machine and a general description of the total system are presented.

D. L. Bernreuter, *A Geophysical Assessment of Near-Field Ground Motion and the Implications for the Design of Nuclear Installations,* Lawrence Livermore Laboratory, Rept. UCRL-79714 (1977). Presented at the CSNI Specialist Meeting on the 1976 Friuli Earthquake and the Antiseismic Design of Nuclear Installations, Rome, Italy, October 11-13, 1977.

This paper gives an in-depth discussion on the various methodologies currently available to predict the near-field ground motion from an earthquake. The limitations of the various methods are discussed in some detail in light of recently available data. It is shown that, (at least for California earthquakes) for an earthquake with a given magnitude a wide variation in the peak ground motion can occur. The change in the spectral content of the ground motion is given as a function of earthquake magnitude and peak ground acceleration. It is shown that the large g values associated with small earthquakes are relatively unimportant in the design provided the structures have a modest amount of ductility.

Data recently obtained from the Friuli earthquake are also examined. Although not all the geophysical data are currently available, the provisional conclusion is reached that the relation between the strong ground motion from this earthquake and its source parameters is the same as for the western United States.

C. L. Hanson, *Thermal-Mechanical Design of a 150-mA, Direct-Current, 400-keV Accelerator for Production of 14-MeV Neutrons,* Lawrence Livermore Laboratory, Rept. UCRL-79721 (1977). To be published in the Proceedings of the Seventh Symposium on Engineering Problems of Fusion Research, Knoxville, Tennessee, October 25-28, 1977.

Several unique accelerator components have been designed and built for the Rotating Target Neutron Source Facility at the Lawrence Livermore Laboratory. Particular consideration was given to material selection and cooling design of components because the facility will have a large steady-state beam energy. Components discussed in this paper include the system composed of the ion source and 90-deg double-focusing magnet in the high-voltage terminal, a water-cooled 400-keV acceleration column, a pyrolytic-graphite beam collimator, and quick-disconnect beam-tube couplings.

S. R. Vosen, D. J. Bender, J. H. Fink, and J. D. Lee, *Mechanical Design Criteria for Continuously Operating Neutral Beams,* Lawrence Livermore Laboratory, Rept. UCRL-79730 (1977). To be published in the Proceedings of the Seventh Symposium on Engineering Problems of Fusion Research, Knoxville, Tennessee, October 25-28, 1977.

Mechanical design criteria for high-energy neutral beam injectors capable of prolonged operation are examined. The generalized structural, heat transfer, and hydraulics equations are presented for convectively cooled grids. The effectiveness of helium, liquid sodium, and subcooled water for

cooling a 2-mm-diameter, 8-m-long grid tube is shown. Cooling effectiveness is determined as a function of the number of tubes in series vs heat flux, where the number of tubes in series ranges from 1 to 100 and the heat flux ranges from 100 to 10,000 W/cm^2. The stress analysis of the grid tube walls is presented, enabling data to be added to the heat transfer graphs and giving an upper flux limit for some grid materials. Sputtering is found to be a possible limiting factor for the grid lifetimes. In injectors designed for continuous use, long-term operation without excessive maintenance is required and sputtering must be minimized. To accomplish this, several procedures are proposed.

F. K. Chen, A. K. Chargin, B. S. Denhoy, and A. F. Waugh, *Design for the Magnetic Field Requirements of the Tandem Mirror Experiment,* Lawrence Livermore Laboratory, Rept. UCRL-79743 (1977). Submitted to the Seventh Symposium on the Engineering Problems of Fusion Research, Knoxville, Tennessee, October 25-28, 1977.

The tandem mirror magnetic geometry is described, followed by an analysis of the magnet set designed to meet the requirements of the TMX experiment. The final magnet line-up is composed of a baseball coil with two C coils for each plug, six solenoidal coils for the central cell, and two RC coils plus one octupole coil for each transition.

R. C. Ling, Y. Chang, and L. D. Hunt, *The MFTF Reel Support,* Lawrence Livermore Laboratory, Rept. UCRL-79747 (1977). To be presented at the Seventh Symposium on Engineering Problems of Fusion Research, Knoxville, Tennessee, October 25-28, 1977.

The MFTF Reel Support has three main functions. It has to support the reel which is 134" in diameter, 40" wide, and can store up to 8,600' of the MFTF superconductor weighing 8,600 lbs. It also serves as a tensioning device for the superconductor with the force of up to 600 lb. Further, it needs to provide vertical and lateral motions for the purpose of facilitating the operation of fabricating MFTF magnets. The support has been designed and is now in fabrication. This paper describes the performance requirements of this device and the evolution of design from conceptual stage to completion.

A. K. Chargin, M. O. Calderon, L. J. Mooney, and G. E. Vogtlin, *System Design for the New TMX Machine,* Lawrence Livermore Laboratory, Rept. UCRL-79749 (1977). To be published in the Proceedings of the Seventh Symposium on Engineering Problems of Fusion Research, Knoxville, Tennessee, October 25-28, 1977.

The Tandem Mirror Experiment (TMX) is designed to test the physics of a new approach to Q-enhancement in open confinement systems. In the tandem mirror concept, the ends of a long solenoid are plugged electrostatically by means of ambipolar potential barriers created in two mirror machines or plugs, one at each end of the solenoid. The ambipolar potential in mirror machines develops as a consequence of the higher scattering rate of electrons and the balancing of electron and ion loss rates.

The TMX experiment incorporates very few new engineering developments, but it does involve a new way of combining in an integrated system many previously developed ideas. The engineering task is to design the machine that would provide a proof-of-principle evaluation of the tandem mirror concept as rapidly as possible. The preliminary design was started in September 1976 and was completed by December 1976. It led to a cost estimate of $11 million and a scheduled construction period of 18 months.

S. R. Thomas, Jr., T. H. Batzer, M. O. Calderon, R. H. Hawkins, and R. J. Nagel, *A Large Rectangular Bellows Valve,* Lawrence Livermore Laboratory, Rept. UCRL-79751 (1977). To be published in the Proceedings of the Seventh Symposium on Engineering Problems of Fusion Research, Knoxville, Tennessee, October 25-28, 1977.

Neutral-beam injection is a primary means of building high-energy plasmas in present mirror fusion machines. The injectors need periodic maintenance while a machine is operating, so isolation of them by valving is a desirable characteristic. Because their energy densities have practical limits, the beams require large cross-sections. Thus, valves having apertures of 10 ft^2 would be common. Traditional cam-seated vacuum gate valves have been built this large, but they are bulky, costly, and heavy. Improvement is possible by use of an inflatable-bellows assembly for the valve gate. This paper describes the design of such a valve. The design allows a clear aperture of 20 by 36 in. with a valve body that is only 5-1/4 in. thick.

R. E. Hinkle, A. R. Harvey, M. O. Calderon, A. K. Chargin, F. F. K. Chen, B. S. Denhoy, J. A. Horvath, J. R. Reed, and A. F. Waugh, *TMX Magnets: Mechanical Design,* Lawrence Livermore Laboratory, Rept. UCRL-79752 (1977). Submitted

to the Seventh Symposium on Engineering Problems of Fusion Research, Knoxville, Tennessee, October 25-28, 1977.

The Tandem Mirror Experiment (TMX) system, part of the Lawrence Livermore Laboratory magnetic mirror program incorporates in its design various types of coils or magnets. This paper describes the physical construction of each coil within the system as well as the structural design required for their support and installation.

M. O. Calderon, F. F. K. Chen, and B. S. Denhoy, *Mechanical Design for TMX Injector System,* Lawrence Livermore Laboratory, Rept. UCRL-79753 (1977). To be published in the Proceedings of the Seventh Symposium on Engineering Problems of Fusion Research, Knoxville, Tennessee, October 25-28, 1977.

The injector system for the Tandem Mirror Experiment (TMX) contains the components required to create and maintain a high-temperature, high-density plasma. These components include a streaming plasma gun in each of the plug tanks to form the target-plasma, 24 neutral-beam source modules for injecting neutral deuterium atoms to heat and replace losses from the plasma, and a gas box system that applies a streaming cold gas to the plasma to stabilize it. This paper discusses the mechanical design problems and solutions for this injector system.

S. R. Thomas, Jr., *TMX, A New Facility,* Lawrence Livermore Laboratory, Rept. UCRL-79754 (1977). To be published in the Proceedings of the Seventh Symposium on Engineering Problems of Fusion Research, Knoxville, Tennessee, October 25-28, 1977.

As a mirror fusion facility, the Tandem Mirror Experiment (TMX) at the Lawrence Livermore Laboratory (LLL) is both new and different. It utilizes over 23,000 ft^2 of work area in three buildings and consumes over 14 kWh of energy with each shot. As a systems design, the facility is broken into discreet functional regions. Among them are a mechanical vacuum pumping system, a liquid-nitrogen system, neutral-beam and magnet power supplies, tiered structures to support these supplies, a neutron-shielded vacuum vessel, a control area, and a diagnostics area. Constraints of space, time, and cost have all affected the design.

D. P. Atkinson and M. O. Calderon, *Liquid Nitrogen Cooled Liners for 2XIIB,* Lawrence Livermore Laboratory, Rept. UCRL-79755 (1977). To be published in the Proceedings of the Seventh Symposium on Engineering Problems of Fusion Research, Knoxville, Tennessee, October 25-28, 1977.

Liquid-nitrogen-cooled liners have been installed in the neutral-beam source tanks of 2XIIB. The installation has resulted in improvements in vacuum pumping, although testing is not complete. The liners are stainless-steel-flooded-type liners, using spot-welded-and-inflation construction. The natural-convection flow system must keep the liners cold during the high heat loads imposed during Ti gettering.

I. F. Stowers, H. G. Patton, W. A. Jones, and D. E. Wentworth, *Techniques for Preventing Damage to High Power Laser Components,* Lawrence Livermore Laboratory, Rept. UCRL-79823 (1977). Presented at the Electro Optics/Laser 77 Conference and Exposition, Anaheim, California, October 25-27, 1977.

The useful life of high power laser disk amplifiers is limited by damage to the optical surfaces. The damage is caused by the rapid heating of contaminant particles on optical surfaces. Initial chemical surface treatments eliminate surface asperities which could become contaminants. A high pressure solvent spray is used to remove all loose particles before assembly and the amplifier is filled with ultra clean dry nitrogen to prevent contamination while in service.

All cleaning and assembly procedures which have evolved to achieve cleanliness levels of 2 particles/cm^2 > 5 μm are described. Design innovations within the amplifier such as elimination of sliding surfaces and screw fasteners minimizes recontamination during assembly. Lifetimes of one year or 500 shots are anticipated based on preliminary tests.

G. A. Carlson, W. C. Condit, R. S. Devoto, and W. S. Neef, *The Field Reversed Mirror Reactor,* Lawrence Livermore Laboratory, Rept. UCRL-80074 (1977). To be published in the Proceedings of IAEA Conference and Workshop on Fusion Reactor Design, University of Wisconsin, Madison, Wisconsin, October 1977.

The parametric analysis and preliminary conceptual design for a multicell field reversed mirror reactor (FRM) are described.

R. W. Moir, W. L. Barr, G. A. Carlson, W. L. Dexter, J. N. Doggett, J. H. Fink, G. W. Hamilton, J. D. Lee, B. G. Logan, W. S. Neef, Jr., M. A.

Peterson, and M. F. Rensink, *The Tandem Mirror Reactor*, Lawrence Livermore Laboratory, Rept. UCRL-80075 (1977). To be published in the Proceedings of the IAEA Conference and Workshop on Fusion Reactor Design, University of Wisconsin, Madison, Wisconsin, October 1977.

A parametric analysis and a preliminary conceptual design for a 1000 MWe Tandem Mirror Reactor (TMR) are described. The concept is sufficiently attractive to encourage further work, both for a pure fusion TMR and a low technology TMR Fusion-Fission Hybrid.

J. A. Horvath, *Using Computer Graphics to Analyze the Placement of Neutral-Beam Injectors for the Mirror Fusion Test Facility*, Lawrence Livermore Laboratory, Rept. UCRL-80106 (1977). To be published in the Proceedings of the Seventh Symposium on Engineering Problems of Fusion Research, Knoxville, Tennessee, October 25-28, 1977.

To optimize the neutral-beam current incident on the fusion plasma and limit the heat load on exposed surfaces of the Mirror Fusion Test Facility magnet coils, impingement of the neutral beams on the magnet structure must be minimized. Also, placement of the neutral-beam injectors must comply with specifications for neutral-current heating of the plasma and should allow maximum flexibility to accommodate alternative beam aiming patterns without significant hardware replacement or experiment down-time. Injector placements and aimings are analyzed by means of the Structural Analysis Movie Post Processor (SAMPP), a general-purpose graphics code for the display of three-dimensional finite-element models. SAMPP is used to visually assemble, disassemble, or cut away sections of the complex three-dimensional apparatus, which is represented by an assemblage of 8-node solid finite elements. The resulting picture is used to detect and quantify interactions between the structure and the neutral-particle beams.

R. H. Toland, *Rotor Design Implications for Composite Material Properties*, Lawrence Livermore Laboratory, Rept. UCRL-80117 (1977). To be published in the Proceedings of the 1977 Flywheel Technology Symposium, San Francisco, California, October 5-7, 1977.

The role and needs of materials research and characterization are defined within the context of the rotor design and analysis process. In particular, we see that material/geometry tailoring permits design optimization, composites can be utilized most efficiently when fiber properties govern rotor performance and reliability, and time-dependent properties are essential for practical and reliable rotor design.

R. W. Werner, *The Cassette Blanket and Vacuum Building: Key Elements in Fusion Reactor Maintenance*, Lawrence Livermore Laboratory, Rept. UCRL-80120 (1977). Submitted to the Seventh Symposium on Engineering Problems of Fusion Research, Knoxville, Tennessee, October 25-28, 1977.

The integration of two concepts important to fusion power reactors is discussed. The first concept is the vacuum building, which improves upon the current fusion reactor designs. Tokamak reactors are complicated, may frequently need repair and are virtually inaccessible for some repairs. A part of the complication arises because the closed surface separating the "hard" vacuum of the plasma zone from atmospheric pressure is located either at the first wall or between the blanket and shield. This surface is subject to radiation damage, cyclic fatigue and loss of function and *in situ* repair is extremely difficult. Enclosing the entire reactor in a vacuum building simplifies and changes the character of this closed surface.

The second concept, the use of the cassette blanket within the vacuum building environment, introduces four major improvements in blanket design:

- *Cassette blanket module*. The key unit for simplification of blanket replacement and maintenance. It also isolates the lithium from the plasma by enveloping it in the coolant.
- *Zoning concept*. Because radiation damage to a structure decreases exponentially with distance, the use of cassettes in series requires only the front fraction of the blanket, the first cassette, be changed as a result of damage during the plant life.
- *Rectangular blanket concept*. Using this geometry, cassettes may be installed or removed by simple linear motion, between toroidal and poloidal coils.
- *Internal tritium recovery*. A favorable temperature gradient is used to diffuse tritium out of the cassette.

R. R. Sandberg, *Design and Testing of a New Multipurpose Tritium Shipping Package*, Lawrence Livermore Laboratory, Rept. UCRL-80122 (1977). To be published in the Proceedings of the DAMSUL Committee, U.S. ERDA Nevada Operations Office, Las Vegas, Nevada, May 18-19, 1977.

J. H. Pitts and E. W. McCauley, *Results from the 1/5-Scale Mark I BWR Pressure Suppression Experiment,* Lawrence Livermore Laboratory, Rept. UCRL-80221 (1977). Presented at the Fifth Water Reactor Safety Research Information Meeting, National Bureau of Standards, Gaithersburg, Maryland, November 7-11, 1977.

A series of consistent, versatile, and accurate air-water tests simulating LOCA conditions has been completed on the 1/5-scale Mark I BWR Pressure Suppression Experimental Facility. Detailed histories of vertical loads on the wetwell are obtained in a carefully scaled three-dimensional system. In particular, variation of hydrodynamic-generated vertical loads with changes in drywell pressurization rate, downcomer submergence, and the vent-line loss coefficient were established. An initial drywell overpressure, which partially preclears the downcomers of water, substantially reduced peak vertical loads.

A. M. Frank, J. B. Bryan, and R. W. Clouser, *Quick, Fast, Off-Axis Parabolas,* Lawrence Livermore Laboratory, Rept. UCRL-80237 (1977). Submitted to *Applied Optics.*

G. E. Cummings, J. E. Wells, and H. E. Lambert. *Assessment of Seismic Trip Systems for Commercial Power Reactors,* Lawrence Livermore Laboratory, Rept. UCRL-80245 (1977). Submitted to the *Nuclear Safety Journal.*

This article assesses the value of seismic trip (scram) systems on commercial nuclear power reactors. Experiences with seismic trip systems on research and test reactors are reviewed as are current regulations concerning seismic instrumentation on power reactors. The advantages and disadvantages of seismic trips are discussed and a comparative risk assessment made using fault tree techniques. The possibility of using a precursor signal from an earthquake to trip the reactor before the arrival of strong motion is also explored.

N. J. Brown, *Optical Polishing Pitch,* Lawrence Livermore Laboratory, Rept. UCRL-80301 (1977). Submitted to the Optical Society of America Workshop on Optical Fabrication and Testing, San Mateo, California, November 10-12, 1977.

This report describes the flow of pitch on polishing laps, discusses the properties of pitch that today appear important, presents some pitch data, and describes pitch testing methods.

N. J. Brown. *Computationally Directed Aspheric Figuring,* Lawrence Livermore Laboratory, Rept. UCRL-80302 (1977). Submitted to the Optical Society of America Workshop on Optical Fabrication and Testing, San Mateo, California, November 10-12, 1977.

A simplified version of wear theory applicable to a wide variety of axisymmetric aspherics is developed. Several programs consistent with programmable hand calculators are presented and a problem is worked in detail.

P. C. Baker, *Polishing and Polishing Materials,* Lawrence Livermore Laboratory, Rept. UCRL-80325 (1977). Submitted to the Optical Society of America Workshop on Optical Fabrication and Testing, San Mateo, California, November 10-12, 1977.

The current approach to optical surface finishing indicates a general dependence on trial and error methods. This paper discusses some of the detailed research that is being done and advances the need for a more scientific approach by the opticians.

REFERENCES

1. J. P. Dow, *Quality Assurance for Systems at the LLL Tritium Facility*, Lawrence Livermore Laboratory, Rept. UCRL-78208 (1976).
2. L. M. Dorfman, B. A. Hemmer, and C. F. Pachucki, *The Interaction of Tritium with Polymeric Materials*, Knolls Atomic Power Laboratory, Idaho Falls, Idaho, Rept. No. KAPL-980 (1953). Also R. W. King, N. J. Broadway, and S. Palinchak, *The Effect of Nuclear Radiation on Elastomeric and Plastic Components and Materials*, Battelle Memorial Institute, Columbus, Ohio, Rept. No. REIC-21 (1961).
3. S. W. Dean, Jr., "Review of Recent Studies on the Mechanism of Stress-Corrosion Cracking in Austenitic Stainless Steels," in *Stress Corrosion—New Approaches* (American Society for Testing Materials, 1976), pp. 308-327.
4. R. J. Billia, *Stain Gages Subjected to a High Pressure Hydrogen Environment*, Lawrence Livermore Laboratory, Rept. UCRL-16908 (1975).
5. H. S. Freynik, Jr., D. R. Roach, D. W. Deis, and D. G. Hirzel, *Nickel-Chromium Strain Gages for Cryogenic Stress Analysis of Superconducting Structures in High Magnetic Fields*, Lawrence Livermore Laboratory, Rept. UCRL-79726 (1977).
6. H. S. Freynik, Jr., D. R. Roach, D. W. Deis, and D. G. Hirzel, "Evaluation of Metal-Foil Strain Gages for Cryogenic Application in Magnetic Fields," Lawrence Livermore Laboratory, Rept. UCRL-79202, to be published in *Adv. Cryogenic Engrg.* **23** (1978).
7. D. W. Deis, D. G. Hirzel, A. R. Rosdahl, D. R. Roach, H. S. Freynik, Jr., and J. P. Zbasnik, "Evaluation of Large, Multifilament Nb_3Sn Conductors With a New 12-Tesla Tensile Test Apparatus," Lawrence Livermore Laboratory, Rept. UCRL-79192, to be published in *Adv. Cryogenic Engrg.* **23** (1978).
8. R. D. Greenough and C. Underhill, "Strain Gauges for the Measurement of Magnetostriction in the Range 4 K to 300 K," in *J. Phys. E: Sci. Instr.* **9**, 451 (1976).
9. P. L. Walstrom, "The Effect of High Magnetic Fields on Metal Foil Strain Gauges at 4.2 K," in *Cryogenics* **15**, 270 (1975).
10. G. Hartwig and F. Wuchner, "Low Temperature Properties of Strain Gauges," in *Materialpruf* **18**(2), 40 (1976). (In German with English abstract and figure titles.)
11. G. M. Ecord, "Composite Pressure Vessels for the Space Shuttle Orbiter," in *Composites in Pressure Vessels and Piping*, S. V. Kulkarni and C. H. Zweben, Eds., ASME publication No. PVP-PB-021 (1977), pp. 129-140; presented at the Energy Technology Conference, Houston, Texas, September 18-23, 1977.
12. E. C. Jessen, H. Spanheimer, and A. J. Herrera, *Prediction of Composite Pressure Vessel Performance by Application of the Kaiser Effect in Acoustic Emission*, presented at ASME Pressure Vessels and Piping Conference, San Francisco, California, June 1975; also corporate paper No. H300-12-2-037 (June 1975), Hercules Incorporated, Systems Division, Magna, Utah, and Thiokol Corporation, Wasatch Division, Brigham City, Utah.
13. M. A. Hamstad and T. T. Chiao, "Structural Integrity of Fiber/Epoxy Vessels by Acoustic Emission," in *SAMPE Quarterly* 8(1), 31 (1976).
14. M. A. Hamstad and R. B. Patterson, "Considerations for Acoustic Emission Monitoring of Spherical Kevlar/Epoxy Composite Pressure Vessels," in *Composites in Pressure Vessels and Piping*, S. V. Kulkarni and C. H. Zweben, Eds., ASME publication No. PVP-PB-021 (1977), pp. 141-163; presented at the Energy Technology Conference, Houston, Texas, September 18-23, 1977.
15. J. P. Mahler and R. T. Bradley, *The LLL Sphere-Winding Machine*, Lawrence Livermore Laboratory, Rept. UCRL-51934 (1975).
16. M. A. Hamstad and T. T. Chiao, "A Physical Mechanism for the Early Acoustic Emission in an Organic-Fiber/Epoxy Pressure Vessel," in *SAMPE Quarterly* 5(2), 22 (1974).
17. D. K. Fisher, M. R. Posehn, F. L. Sindelar, and H. H. Bell, *Computer-Based Transportable Data-Acquisition and Control System*, Lawrence Livermore Laboratory, Rept. UCRL-78339 (1976). Presented at the 45th Shock and Vibration Symposium, Albuquerque, New Mexico, October 19-21, 1976.
18. M. R. Posehn, *Modal Analysis of the NRC Pressure Suppression Experimental Facility*, Lawrence Livermore Laboratory, Rept. UCID-17494 (1977).
19. R. Potter, "A General Theory of Modal Analysis for Linear Systems," in *Shock and Vibration Digest* 7(11) (1975).

20. A. Klosterman and R. Zimmerman, *Modal Survey Activity Via Frequency Response Functions*, Society of Automotive Engineers National Aerospace Engineering and Manufacturing Meeting Paper No. 751068 (Society of Automotive Engineers, Warrendale, Pennsylvania, 1976).
21. A. Klosterman, W. A. McClelland, and J. E. Sherlock, *Dynamic Simulation of Complex Systems Utilizing Experimental and Analytical Techniques*, presented at the ASME Aerospace Division Winter Annual Meeting, Houston, Texas, December 4, 1975 (Paper No. ASME 75-WA/Aero-9).
22. M. Richardson and K. A. Ramsey, "Making Effective Transfer Function Measurements for Modal Analysis," in *Proceedings of the Institute of Environmental Sciences, 1976* (Institute of Environmental Sciences, Mount Prospect, Illinois, 1977).
23. G. R. Gather, J. W. Shaner, C. A. Calder, and W. W. Wilcox, "Determination of Sound Velocity in Liquid Metals at Temperatures Greater than 4000 K," in *Proc. Seventh Symposium Thermophysical Properties, May 10-12, 1977* (National Bureau of Standards, Gaithersburg, MD, 1977).
24. E. Schreiber, L. A. Orson, and N. Soga, *Elastic Constants and Their Measurement* (McGraw-Hill, New York, 1973).
25. C. A. Calder and W. W. Wilcox, "Technique for Measurement of Elastic Constants by Laser Energy Deposition," in *Rev. Sci. Instru.* **45**(12), 1557 (1974).
26. C. A. Calder and W. W. Wilcox, *Acoustic Velocity Measurement Across the Diameter of a Small Rod*, Lawrence Livermore Laboratory, Rept. UCRL-78751 (1976).
27. G. Simmons and H. Wang, *Single Crystal Elastic Constants and Calculated Aggregate Properties: A Handbook, 2nd Ed.* (MIT Press, Cambridge, 1971).
28. G. M. B. Webber and R. W. B. Stephens, "Transmission of Sound in Molten Metals," in *Physical Acoustics*, W. O Mason, Ed., Vol. IV-Part B (Academic Press, New York, 1968), pp. 53-97.
29. For a more complete report of the instrumentation for this experiment see: W. Shay, W. Brough, and T. Miller, *Instrumenting a Pressure Suppression Experiment for a Mark I Boiling Water Reactor—Another Measurements Engineering Challenge*, Lawrence Livermore Laboratory, Rept. UCRL-52314 (1977).

MBB